

Superconducting tetrahedral quantum bits

M.V. Feigel'man¹, L.B. Ioffe^{2,1}, V.B. Geshkenbein^{3,1}, P. Dayal³, and G. Blatter³

¹*Landau Institute for Theoretical Physics, 117940 Moscow, Russia*

²*Department of Physics and Astronomy, Rutgers University, Piscataway, NJ 08854, USA and*

³*Theoretische Physik, ETH-Hönggerberg, CH-8093 Zürich, Switzerland*

(Dated: November 14, 2018)

We propose a new design for a quantum bit with four superconducting islands in the topology of a symmetric tetrahedron, uniformly frustrated with one-half flux-quantum per loop and one-half Cooper-pair per island. This structure emulates a noise-resistant spin-1/2 system in a vanishing magnetic field. The tetrahedral quantum bit combines a number of advances such as a doubly degenerate ground state minimizing decoherence via phonon radiation, a weak quadratic sensitivity to electric and magnetic noise, relieved constraints on the junction fabrication, a large freedom in manipulation, and attractive measurement schemes. The simultaneous appearance of a degenerate ground state and a weak noise sensitivity are consequences of the tetrahedral symmetry, while enhanced quantum fluctuations derive from the special magnetic frustration. We determine the spectral properties of the tetrahedral structure within a semiclassical analysis and confirm the results numerically. We show how proper tuning of the charge-frustration selects a doubly degenerate ground state and discuss the qubit's manipulation through capacitive and inductive coupling to external bias sources. The complete readout of the spin-components σ_i , $i = x, y, z$, is achieved through coupling of the internal qubit currents to external junctions driven close to criticality during the measurement.

I. INTRODUCTION

Superconducting solid-state qubits (short for quantum bits) are promising candidates for the future construction of quantum information processors. They appear in a variety of designs: in the charge-version^{1,2,3} the quantum information is stored in the number of excess Cooper pairs residing on a small superconducting island — this design requires fabrication of ultra-small structures and is susceptible to charge noise. In the flux-⁴ and phase-^{5,6} versions the information is encoded in the current state of the device — this is a macroscopic variable susceptible to flux noise. The new design by Vion *et al.*⁷ is ‘in between’, with the energy scales for the charge- ($E_C = e^2/2C$) and the phase- ($E_J = \Phi_0 I_c/2\pi c$) degrees of freedom roughly balancing one another (here, C and I_c are the capacitance and the maximal current of the device, $\Phi_0 = hc/2e$ is the flux quantum); its ground state is non-degenerate and the limitations are close to those of the charge device.

The novel tetrahedral qubit design we propose below operates in the phase-dominated regime and exhibits two remarkable physical properties: first, its non-Abelian symmetry group (the tetrahedral group T_d) leads to the natural appearance of degenerate states and appropriate tuning of parameters provides us with a doubly degenerate groundstate. Our tetrahedral qubit then emulates a spin-1/2 system in a vanishing magnetic field, the ideal starting point for the construction of a qubit. Manipulation of the tetrahedral qubit through external bias signals translates into application of magnetic fields on the spin; the application of the bias to different elements of the tetrahedral qubit corresponds to rotated operations in spin space. Furthermore, geometric quantum computation via Berry phases^{8,9} might be implemented through adiabatic change of external variables. Going one step

further, one may hope to make use of this type of systems in the future physical realization of non-Abelian anyons, thereby aiming at a new generation of topological devices^{10,11,12,13} which keep their protection even during operation¹⁴.

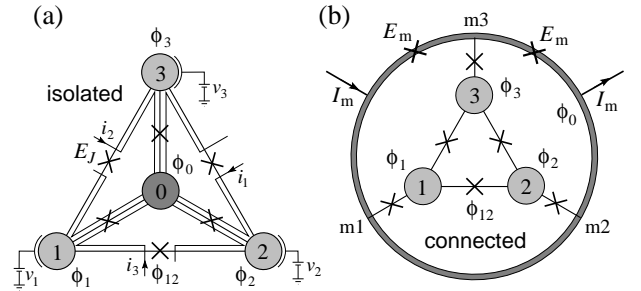


FIG. 1: (a) Tetrahedral superconducting qubit involving four islands and six junctions (with Josephson coupling E_J and charging energy E_C); all islands and junctions are assumed to be equal and arranged in a symmetric way. The islands are attributed phases ϕ_i , $i = 0, \dots, 3$. The qubit is manipulated via bias voltages v_i and bias currents i_i . In order to measure the qubit's state it is convenient to invert the tetrahedron as shown in (b) — we refer to this version as the ‘connected’ tetrahedron with the inner dark-grey island in (a) transformed into the outer ring in (b). The measurement involves additional measurement junctions with couplings $E_m \gg E_J$ on the outer ring which are driven by external currents I_m (schematic, see Fig. 6 for details); the large coupling E_m effectively binds the ring segments into one island.

The second property we wish to exploit is geometric frustration: In our tetrahedral qubit discussed below it appears in an extreme way by rendering the classical minimal states continuously degenerate along a line in parameter space. Semi-classical states then appear

only through a fluctuation-induced potential, reminiscent of the Casimir effect¹⁵ and the concept of inducing ‘order from disorder’^{16,17}. The quantum-tunneling between these semi-classical states defines the operational energy scale of the qubit, which turns out to be unusually large due to the weakness of the fluctuation-induced potential. Hence the geometric frustration present in our tetrahedral qubit provides a natural boost for the quantum fluctuations without the stringent requirements on the smallness of the junction capacitances, thus avoiding the disadvantages of both the charge- and the phase-device: The larger junctions reduce the demands on the fabrication process and the susceptibility to charge noise and mesoscopic effects, while the large operational energy scale due to the soft fluctuation-induced potential reduces the effects of flux noise. Both types of electromagnetic noise, charge- and flux noise, appear only in second order (cf. also Ref. 7).

In the following (Sec. 2), we first introduce the structure of our tetrahedral qubit and then find the low-energy part of its spectrum. We proceed in three steps, beginning with the (highly degenerate) classical solution; subsequently, we demonstrate how the fluctuation induced potential reduces this degeneracy to three semi-classical states and finally, we analyze the tunneling between them in order to arrive at the final answer for the phase dominated regime. We confirm this solution with the help of numerical calculations and extend it to the charge dominated regime. The inclusion of external fields breaking the (tetrahedral) symmetry of the device prepares the discussion of the qubit’s manipulation schemes (section 3). In section 4, we discuss various measurement schemes and end with the conclusions in Sec. 5. A first account on part of this work has been given in Ref. 18.

II. TETRAHEDRON

A. Device structure

Consider the planar structure made from four superconducting islands interconnected via six (conventional) Josephson junctions with equal couplings E_J ; connecting each island with all the others produces the topology of a tetrahedron, see Fig. 1(a). The islands are numbered through ‘0’ to ‘3’, with the island ‘0’ residing in the center, and are assigned phases ϕ_i , $i = 0, \dots, 3$. The three triangular loops are small (i.e., $E_J \ll (\Phi_0/2\pi)^2/L_\Delta$ with L_Δ the loop inductance), allowing us to neglect fluxes induced by currents flowing in the structure. In the absence of external magnetic fields, the classical energy of this arrangement is given by the sum $V_0 = \sum_{i<j} E_J [1 - \cos(\phi_{ij})]$ with the difference variables $\phi_{ij} = \phi_j - \phi_i$. A slightly modified version of this device with the inner island converted into an enclosing ring is shown in Fig. 1(b) — choosing appropriate parameters, this variant exhibits the same physical properties as the original isolated tetrahedral qubit. In addition, this second design ideally

lends itself for measurement of the qubit state. Below, we treat the ring as one connected island; the strong junctions with $E_m \gg E_J$ used in the measurement process will be discussed later.

Next, we bias the structure through an external magnetic field, frustrating each sub-loop with a flux $\Phi_0/2$ (these are three triangular sub-loops in the isolated version of Fig. 1(a) and 4 sub-loops in the connected version of Fig. 1(b)). We include the effect of this flux in a symmetric gauge by adding the phase π to each of the difference variables ϕ_{ij} ; the energy (up to a trivial constant; we measure phases with respect to the phase ϕ_0 of the central/ring island)

$$V_\pi = E_J [\cos \phi_1 + \cos \phi_2 + \cos \phi_3 + \cos(\phi_3 - \phi_2) + \cos(\phi_1 - \phi_3) + \cos(\phi_2 - \phi_1)] \quad (1)$$

then is minimized (with $V_\pi = -2E_J$) along the lines

$$\phi_3 = \pm\pi; \quad \phi_2 - \phi_1 = \pm\pi; \quad \psi_3 = \phi_1 + \phi_2 \in [-\pi, \pi] \quad (2)$$

and their analogs obtained by cyclic permutation $3 \rightarrow 1 \rightarrow 2 \rightarrow 3$. These minimal-energy lines run in the planes of the cube $[-\pi, \pi]^3$ defined in phase space $\{\phi_1, \phi_2, \phi_3\}$, see Fig. 2(a). The huge (linear) classical degeneracy can be easily understood via a reformulation of the potential (1) in terms of the complex variables $z_k = \exp(i\phi_k)$, $2V_\pi = E_J [|\sum_{k=0}^3 z_k|^2 - 4]$; this expression is minimal for $\sum_k z_k = 0$. The two conditions defined by this (complex) equation imply that one out of the three variables ϕ_k can be freely chosen, thus defining lines of minimal potential energy. Of particular relevance are the minimal energy configurations O_i , $i = 1, 2, 3$ on the cube edges where two minimal-energy lines join. These configurations involve two opposite junctions with a phase difference $\phi_{ij} = 0$, while the remaining junctions involve maximal phase differences π ; following three consecutive segments on the cube, these minimal states rotate through 2π , see Fig. 2(a) (here, we have included the bias phases π on each link; in the original variables these states involve 2 strained junctions with phase difference π and 4 unstrained ones with phase difference 0; note the absence of currents in these configurations).

We account for the quantum dynamics in the array via the capacitive term

$$T = \frac{\hbar^2}{4e^2} \left[\sum_{i<j} \frac{C_J}{2} (\dot{\phi}_{ij})^2 + \sum_{i=1}^3 \frac{C_g}{2} (\dot{\phi}_i)^2 + \frac{C_0}{2} (\dot{\phi}_0)^2 \right] \quad (3)$$

in the Lagrangian $\mathcal{L} = T - V_\pi$; here, C_J denotes the capacitance of the junctions, while C_g and C_0 are the capacitances to the ground of the islands $i = 1, 2, 3$ and of the center/ring island. An additional term $\hbar \sum_i q_i \dot{\phi}_i$ appears when charges $2eq_i$ are induced on the islands; we will discuss the effect of this topological term later. For the isolated tetrahedron of Fig. 1(a) we have $C_0 = C_g$; going over to center of mass ($4\Phi = \sum_i \phi_i$) and relative coordinates ($\tilde{\phi}_i = \phi_i - \Phi$) the difference variables $\tilde{\phi}_{ij} = \phi_{ij}$

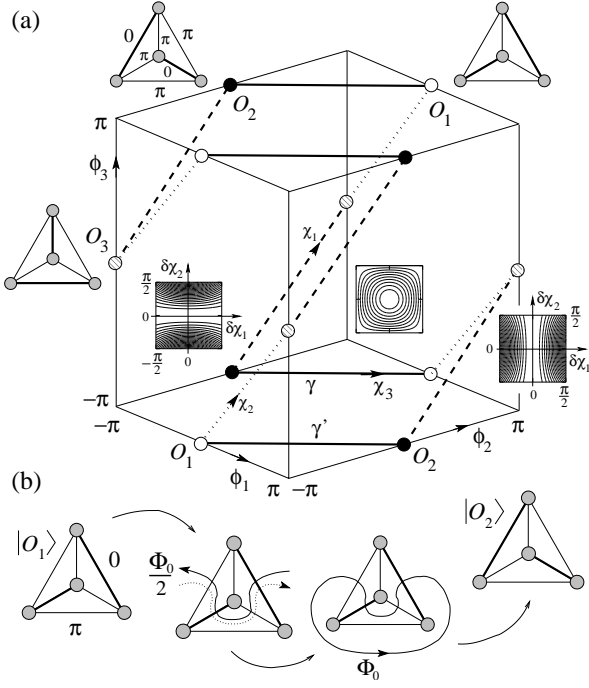


FIG. 2: (a) Continuous degeneracy of the classical minimal energy states. We identify 3 highly symmetric minimal states O_i , $i = 1, 2, 3$ (white, black, and grey dots) involving two opposite junctions with a phase difference $\phi_{ij} = 0$ and four remaining junctions with $\phi_{ij} = \pi$. Three families of lines (solid, dashed, dotted) connect these states around the cube $[-\pi, \pi]^3$ where the energy is continuously degenerate with a value $V_\pi = -2E_J$. The (non-orthogonal) coordinates χ_i are directed along the minima, e.g., $\chi_1 = 0$, $\chi_2 = -\pi$, $\chi_3 \in [0, \pi]$ along the reference line γ along which the change in the potential V_π is shown for the values $\chi_3 = 0, \pi/2, \pi$. Quantum fluctuations induce potential barriers along the minimal lines, separating the classical states O_i and transforming them into semi-classical states $|O_i\rangle$. (b) Tunneling between the states $|O_i\rangle$ establishes the low-energy spectrum of the tetrahedron. The tunneling process connecting the states $|O_1\rangle$ and $|O_2\rangle$ involves two trajectories γ and γ' where a fluxon $\Phi_0/2$ cuts through 4 junctions, flipping all of them by π . The phase difference between the two trajectories (the solid line corresponds to γ) produces the Aharonov-Bohm-Casher phase obtained when taking the fluxon Φ_0 around the islands ‘1’ and ‘2’.

pick up an additional capacitance $C_0/4$ and the corresponding part of the kinetic energy can be written in the form $T_{\text{rel}} = (\hbar^2/16E_C) \sum_{i<j} \dot{\phi}_{ij}^2$, with the capacitive energy $E_C = e^2/2C$ and $C = C_J + C_0/4$. The identical expression for the kinetic energy is obtained for the inverted tetrahedron in Fig. 1(b) if we choose a large self-capacitance $C_0/C_J \rightarrow \infty$ for the ring and a small one $C_g/C_J \rightarrow 0$ for the other islands, then $E_C = e^2/2C_J$; this limit describes the inverted tetrahedron connected to the outside world via (large) superconducting wires fixing the phase $\phi_0 = 0$. The following discussion applies to both designs of Fig. 1; we first assume that $E_C \ll E_J$, placing the array into the phase-dominated regime.

B. Semi-classical Analysis

Next, we account for quantum fluctuations associated with the degenerate line-minima. It is convenient to introduce the (non-orthogonal) variables $\chi_k = (\phi_i + \phi_j - \phi_k)/2$ with $i, j, k \in \{1, 2, 3\}$ and mutually different, where both the kinetic and potential energy terms acquire a simpler form, $T_{\text{rel}} = (\hbar^2/4E_C)[\dot{\chi}_1^2 + \dot{\chi}_2^2 + \dot{\chi}_3^2]$ and $V_\pi = 2E_J[\cos \chi_1 \cos \chi_2 + \cos \chi_1 \cos \chi_3 + \cos \chi_2 \cos \chi_3]$. The new coordinates are directed along the potential minima which are parametrized by fixing two coordinates to 0 and $\pm\pi$ and have the third run through the interval $[0, \mp\pi]$; e.g., the reference line (denoted by γ) connecting O_2 with O_1 in Fig. 2(a) is parametrized by $\chi_1 = 0$, $\chi_2 = -\pi$, $\chi_3 \in [0, \pi]$. In the vicinity of γ the potential energy takes the form $V_\pi \approx E_J[-2 + \delta\chi_1^2(1 - \cos \chi_3) + \delta\chi_2^2(1 + \cos \chi_3)]$; the two fast oscillatory modes χ_1 and χ_2 appear with a curvature which depends on the adiabatic coordinate $\chi = \chi_3$, see Fig. 2(a). Their zero-point fluctuations produce an induced potential

$$V_f(\chi) = \frac{1}{2}[\hbar\omega_1(\chi) + \hbar\omega_2(\chi)], \quad (4)$$

with the frequencies of the fast modes

$$\omega_{1,2}(\chi) = \omega_f \sqrt{[1 \pm \cos(\chi)]/2} \quad (5)$$

and the frequency scale $\omega_f = \sqrt{8E_J E_C}/\hbar$. Near the edges $\chi = 0, \pi$ one of the modes goes to zero, as is clear from the potential shape shown in Fig. 2(a), and we have to refine our analysis. We then remain with only one fast and two slow modes. Expanding V_π around the point $O_2 = (0, -\pi, 0)$ (in χ_i coordinates) we arrive at the potential $V_\pi = (E_J/2)[-4 + 4\delta\chi_2^2 + \delta\chi_1^2\delta\chi_3^2 - \delta\chi_2^2(\delta\chi_1^2 + \delta\chi_3^2)]$; integration over the fast mode χ_2 and transformation to momenta provides us with the Hamiltonian

$$\mathcal{H}_f \approx -E_C \left[\frac{d^2}{d\chi_1^2} + \frac{d^2}{d\chi_3^2} \right] + E_J \frac{\delta\chi_1^2 \delta\chi_3^2 - \kappa(\delta\chi_1^2 + \delta\chi_3^2)}{2}, \quad (6)$$

where $\kappa = \langle \delta\chi_2^2 \rangle = (E_C/8E_J)^{1/2}$. Dimensional analysis tells that the low lying levels of this quartic anisotropic oscillator are of the order of

$$\Omega \equiv \omega_f \left(\frac{E_C}{E_J} \right)^{1/6} \ll \omega_f; \quad (7)$$

the numerical factors determining the exact positions of the groundstate and of the non-equidistant higher levels have to be determined numerically and the results are summarized in Table I; the groundstate energy is accurately described by the expression $\Omega_0/\Omega \approx 0.311 - 0.129(E_C/E_J)^{1/6}$, where the scale dependence of the correction easily follows from first order perturbation theory in the term $-E_J\kappa(\delta\chi_1^2 + \delta\chi_3^2)/2$.

Repeating this analysis for the other classical line-minima, we arrive at three distinct quantum states $|O_i\rangle$ (at energies $-2E_J + \hbar\omega_f/2 + \hbar\Omega_0$) associated with the

TABLE I: Ground- and excited states energies near the minima O_i . The first excited state at Ω_1 is doubly degenerate. The parameter $\nu = \nu_{\#}(E_J/E_C)^{1/3}$ quantifies the susceptibility of the semi-classical ground states $|O_i\rangle$ to applied fluxes, cf. (23).

E_J/E_C	Ω_0/Ω	Ω_1/Ω	Ω_2/Ω	$\nu_{\#}$
∞	0.311	0.70	0.99	1.00
1000	0.271	0.57	0.69	1.23
100	0.250	0.51	0.58	1.53
10	0.225	0.40	0.43	2.50

three classical zero-current states O_i described above. These isolated quantum states are generated through a fluctuation-induced potential reminding about the Casimir force between metallic plates¹⁵ or the van der Waals interaction between neutral atoms¹⁹. This is just the mechanism producing order from disorder originally proposed by Villain^{16,17} where the huge classical ground state degeneracy (which does not follow from the symmetry properties of the system) is removed by quantum fluctuations, here, selecting the three points $|O_i\rangle$ as new ground states.

The low-energy spectrum near the points O_i exhibits non-equidistant levels Ω_i even deep in the semiclassical regime, allowing for the use of the tetrahedral structure as a simple Josephson junction qubit of the type introduced in Refs. 20,21. Moreover, both symmetry arguments and the numerical data tell that the first excited level is twofold degenerate, such that we effectively deal with a spin 1 system with an easy-plane anisotropy $H_{S=1} = (\Omega_1 - \Omega_0)S_z^2$.

Before going to the full quantum description, let us discuss the above semiclassical version of the device, as it exhibits a number of interesting features by itself. First, the potential (4) defines a doubly-periodic junction²⁴ with two distinct minima. The potential $V_f(\chi)$ can be mapped out experimentally through the measurement of the Josephson current $I_J(\chi)$ that can be pushed through the structure. E.g., fixing the phase ϕ_2 between the central island and the island ‘2’ via a flux-biased external loop defines the two classical minimal solutions $(\phi_2 - \pi, 0, \pi)$ and $(0, -\pi, \phi_2)$ (in χ_i -coordinates). The running coordinate $\chi = \chi_1$ or $\chi = \chi_3$ is equal to ϕ_2 (up to a trivial shift) and thus related to the external bias flux Φ via $\chi = -2\pi\Phi/\Phi_0$. The current $I = -c\partial_\Phi E$ then is given by the expression $I_J(\chi) = (2e/\hbar)\partial_\chi V_f(\chi)$ and is double periodic in the interval $0 \leq \Phi < \Phi_0$ (we define the charge of the electron as $-e$ and $e > 0$). Alternatively, one may measure the frequencies $\omega_{1,2}(\chi)$, cf. Eq. (5), directly via the resonant absorption of an ac -signal.

At nonzero temperatures (but still $T \ll E_J$) the induced potential is driven thermally and involves the free

energy of the two fast oscillating modes,

$$F_f(\chi, T) = \sum_{i=1}^2 \left[\frac{\hbar\omega_i(\chi)}{2} + T \log \left(1 - e^{-\hbar\omega_i(\chi)/T} \right) \right]. \quad (8)$$

Thermal fluctuations become relevant for temperatures $T > \hbar\omega_f$ and lead to an increase in the barrier $\delta F_f(T) \equiv F_f(\pi/2, T) - F_f(0, T)$,

$$\delta F_f(T) = (\hbar\omega_f/2)[\sqrt{2} - (1 + 2\Omega_0/\omega_f)] + T \log[\omega_f/2\Omega_0]. \quad (9)$$

As a result, rather than decreasing, the phase stiffness in the tetrahedron increases with temperature and hence the Josephson current $I_J(T) \propto \partial_\Phi F_f(\Phi, T)$ increases with temperature until the fluctuation-induced potential disappears due to level broadening: thermally induced quasiparticles produce a level broadening $\hbar/RC \sim (E_J E_C/\hbar\Delta) \exp(-\Delta/T)$, where we have used the Ambegaokar-Baratoff relation $I_c R \sim \Delta/e$. This broadening should remain small on the scale of the level separation $\hbar\omega_f$, from which we obtain the condition that $T < \Delta/\ln(\hbar\omega_f/\Delta)$. Beyond this temperature, the Josephson current is expected to decrease again, resulting in a non-monotonic behavior of $I_J(T)$.

In order to arrive at a fully quantum mechanical description of the tetrahedron, we have to account for the tunneling processes between the points O_i , cf. Fig. 2. It is important to note that each set of 4 mid-edge points residing in one plane $\phi_i = 0$ has to be identified with one quantum mechanical state $|O_i\rangle$; on the other hand, the pair of classically degenerate lines connecting two states $|O_i\rangle$ and $|O_j\rangle$ in one of the faces describe different tunneling trajectories, which have to be added coherently in order to arrive at the tunneling matrix element between the two states (the other two trajectories on the opposite face are equivalent). Let us concentrate on the tunneling process between $|O_1\rangle$ and $|O_2\rangle$; the two tunneling trajectories follow the lines parametrized by $\chi_1, \chi_2 \in \{0, -\pi\}$, $\chi_3 \in [0, \pi]$, see Fig. 2(a). The tunneling processes described by these two trajectories flip the phase across the four junctions ‘31’, ‘01’, ‘02’, and ‘23’ by $\pm\pi$, which corresponds to a fluxon $\Phi_0/2$ traversing the tetrahedron as shown in Fig. 2(b) (the same arguments apply to the connected tetrahedron). The phase difference between the two trajectories then corresponds to taking a full fluxon Φ_0 around the two islands ‘1’ and ‘2’, which translates into the Aharonov-Bohm-Casher phase $\exp[2\pi i(q_1 + q_2)]$, with q_i the charge on the island ‘ i ’ measured in units of $2e$ (see Ref. 22 for a detailed discussion of charge-induced interference effects in small superconducting structures; these phases are generated by the topological term $\hbar \sum_i q_i \dot{\phi}_i$ in the Lagrangian \mathcal{L} in the presence of charges $2eq_i$, cf. the note below (3)). Combining this phase factor with the modulus $|a|$ we arrive at the tunneling amplitude

$$t_{12} = -2|a| \cos[\pi(q_1 + q_2)] \quad (10)$$

between the states $|O_1\rangle$ and $|O_2\rangle$; a similar analysis provides the amplitudes for all the other pairs. In the absence of any charge frustration (i.e., for integer charge q_i on each island) the system gains energy from hopping and hence $t < 0$, thus defining the sign in (10). The modulus $|a|$ of the tunnelling amplitude follows from the semi-classical description of the one-dimensional motion under the barrier $V_f(\chi)$ as given by Eq. (4) and takes the form $|a| \approx [\hbar/T(\Omega_0)] \exp[-S_f(\Omega_0)]$, with $T(\Omega_0)$ the classical period of motion and $S_f(\Omega_0)$ the dimensionless action²³, both evaluated at the ground state energy $\hbar\Omega_0$,

$$S_f = \left(\frac{32E_J}{E_C}\right)^{1/4} \int_0^{\chi_0} d\chi [\sqrt{2} \cos(\chi/2) - 1 - 2\Omega_0/\omega_f]^{1/2} \\ \sim 1.88 \left(\frac{E_J}{E_C}\right)^{1/4}, \quad (E_J/E_C)^{1/4} \gg 1, \quad (11)$$

$$T = \frac{8\hbar}{E_J} \left(\frac{\sqrt{2}\Omega_0}{\Omega}\right)^{1/2} \left(\frac{E_J}{E_C}\right)^{2/3}, \quad (12)$$

where $\chi_0 = 2 \arccos[(1+2\Omega_0/\omega_f)/\sqrt{2}]$. The semi-classical analysis describing tunneling at the correct ground state energy $\hbar\Omega_0$ gives very accurate results, see below; the simple asymptotic form (11) describes tunneling from the bottom of the well and is valid only deep in the quasi-classical regime. The result obtained here for the tetrahedron is smaller than the usual tunneling action $S \propto (E_J/E_C)^{1/2}$ of a Josephson junction device involving only the square root of the parameter E_J/E_C ; the unconventional dependence on the ratio E_J/E_C is a consequence of the fluctuation-induced (rather than classical) barrier and puts less stringent requirements (e.g., with respect to the smallness of the junction) on the fabrication process of this new type of qubits.

The above tunneling action can be probed via a measurement of the current-voltage characteristic of the device: applying a fixed bias current across two islands, a finite voltage appears due to quantum and thermally induced phase slips. At low temperatures the appearance of quantum phase slips involves the finite action $S_{ps} = 2\hbar S_f$ and results in an exponentially small resistivity $R \propto \exp(-2S_f)$. At higher temperatures $T > U_{ps}\hbar/S_{ps}$ the phase slips are created thermally via activation over the barrier $U_{ps} = \delta F_f$. The phase-slip induced resistivity then exhibits an unconventional saturation at high temperatures: increasing T beyond $\hbar\omega_f(E_C/E_J)^{1/4}$, the resistivity first increases with temperature. As $T > \hbar\omega_f$ the barrier δF_f itself increases linearly in T and the further rise of R saturates at a value $R \propto \Omega_0/\omega_f$; hence care has to be taken not to confuse the saturation in R at high temperatures with the (exponentially small) quantum resistance surviving as $T \rightarrow 0$.

Let us return to the quantum description of our tetrahedron and study its low-energy spectrum as determined by the quantum coherent oscillations between semi-classical states $|O_i\rangle$; the appearance of the island charges $2eq_i$ in the tunneling amplitudes t_{ij} manifests itself in this level structure. Assuming a uniform distribution of

the total charge $2eq$ on the isolated tetrahedron, the matrix elements take the form $t_{ij} = t = -2|a| \cos(\pi q/2)$ and we have to diagonalize the matrix

$$H_O = \begin{pmatrix} 0 & t & t \\ t & 0 & t \\ t & t & 0 \end{pmatrix}. \quad (13)$$

Depending on the value of q , the low-energy spectrum of the isolated tetrahedron splits into singlets and doublets involving the energies $E_s = 2t$ and $E_d = -t$, or remains tri-fold degenerate with $E_t(t=0) = 0$ (here, energies are measured with respect to the unperturbed value $-2E_J + \hbar(\omega_f/2 + \Omega_0)$); the ground state is a

$$\begin{aligned} \text{singlet if } & q = 4k, \quad \text{even,} \\ \text{doublet if } & q = 4k + 2, \quad \text{even,} \\ \text{triplet if } & q = 2k + 1, \quad \text{odd.} \end{aligned} \quad (14)$$

In the connected tetrahedron of Fig. 1(b) the charge is not quantized on the inner islands; however, the dependence (10) of the tunneling amplitude on the island charges q_i remains valid and the above spectrum is recovered under appropriate biasing of the inner islands with either zero, one-quarter, or one-half Cooper-pair. Biasing the tetrahedron into the charge state $q_i = 1/2$ then establishes a ground state doublet with eigenstates

$$\begin{aligned} |+\rangle &= [|O_1\rangle + \zeta|O_2\rangle + \zeta^*|O_3\rangle]/\sqrt{3}, \\ |-\rangle &= [|O_1\rangle + \zeta^*|O_2\rangle + \zeta|O_3\rangle]/\sqrt{3}, \end{aligned} \quad (15)$$

suitable for the implementation of a quantum bit; here, $\zeta = \exp(2\pi i/3)$. These degenerate states (15) involve bonds resonating with opposite chirality in the device, see Fig. 2(a), and are reminiscent of the resonating dimer bonds in the topologically protected qubits discussed in Refs. 10,11. Also, such chiral states appear as degenerate spin-singlet ground states in the vanadium tetrahedron of the pyrochlore system²⁵. The doublet $|\pm\rangle$ is protected by the gap $\Delta_d = 3t$, separating it from the next excited (singlet) state

$$|0\rangle = [|O_1\rangle + |O_2\rangle + |O_3\rangle]/\sqrt{3}. \quad (16)$$

Combining the results (10), (11), and (12) we obtain the protective and operational energy scale t of the qubit,

$$\frac{t}{E_J} = \frac{1}{4} \left(\frac{\Omega}{\sqrt{2}\Omega_0}\right)^{1/2} \left(\frac{E_C}{E_J}\right)^{2/3} \exp[-S_f(\Omega_0)]. \quad (17)$$

C. Charge limit

We briefly extend our analysis to the charge-dominated regime with $E_C \gg E_J$. It is convenient to go over to a Hamiltonian description; starting from the above Lagrangian (cf. Eqs. (1) and (3)) and eliminating the variable ϕ_0 one obtains the expression

$$H = E_C[\bar{Q}_1^2 + \bar{Q}_2^2 + \bar{Q}_3^2 + (\bar{Q}_1 + \bar{Q}_2 + \bar{Q}_3)^2] \\ + V_\pi(\phi_1, \phi_2, \phi_3), \quad (18)$$

where $\bar{Q}_i = -i\partial_{\phi_i} - q_i$ and q_i is the induced charge on the i -th island (in units of $2e$), $q_i = \sum_j C_{ij}V_j$ for the connected tetrahedron, while an additional term $[q - (C/4)\sum_j V_j]/4$ with $C = \sum_{ij} C_{ij}$ the total capacitance, has to be added for the isolated tetrahedron²² (here, C_{ij} denotes the capacitance matrix, see (3), and V_i are the bias potentials applied to the islands). For the isolated tetrahedron the total charge $q = \sum_0^3 q_i$ is integer, while the total induced charge $q = \sum_1^3 q_i$ can take any value in the connected device. The Hamiltonian (18) describing both devices becomes identical under symmetric bias and for specific values $q_i = k/4$ with k an integer; under these conditions the maximal symmetry S_4 , i.e., the tetrahedral symmetry T_d , is established. Note that a symmetric bias with equal charges $q_i = q/3$ on the three inner islands of the connected tetrahedron in general guarantees only for a S_3 symmetry.

We determine the spectrum for the uniformly charged isolated tetrahedron with $q = 4k + 2$. In the limit $E_C \gg E_J$ the operators \bar{Q}_i take on integer values and the charging term is minimized by distributing two bosons onto the four sites avoiding double occupancy (in this limit, the term $E_C(\bar{Q}_1 + \bar{Q}_2 + \bar{Q}_3)^2$ in (18) describes the charging energy $E_C\bar{Q}_0^2$ of the middle island). The resulting six states ‘01’, ‘02’, ‘03’, ‘23’, ‘31’, and ‘12’ are degenerate with an energy $E_0 = 2E_C$. The hopping term V_π lifts this degeneracy through the mixing via the Josephson coupling E_J : each state ‘ ij ’ hosting Cooper-pairs on the islands ‘ i ’ and ‘ j ’ exchanges particles with all other states except for ‘ kl ’, where $k, l \neq i, j$. The Hamiltonian describing the mixing of the six two-Boson states may be written as a matrix product

$$H_{2B} = \begin{pmatrix} 0 & \tilde{t} & \tilde{t} \\ \tilde{t} & 0 & \tilde{t} \\ \tilde{t} & \tilde{t} & 0 \end{pmatrix} \otimes \begin{pmatrix} 1 & 1 \\ 1 & 1 \end{pmatrix}, \quad (19)$$

where the sign of the tunneling amplitude $\tilde{t} = E_J/2 > 0$ is positive for our frustrated tetrahedron (again, we choose a symmetric gauge with all Josephson couplings reversed in sign). The eigenvalues of the direct matrix product in (19) are given by the product of the eigenvalues $(2\tilde{t}, -\tilde{t}, -\tilde{t})$ of its first factor and those of the second factor, $(0, 2)$; correspondingly we find the first 6 levels at the energies

$$\begin{aligned} E_d &= -E_J && \text{doublet,} \\ E_t &= 0 && \text{triplet,} \\ E_s &= 2E_J && \text{singlet.} \end{aligned} \quad (20)$$

The first excitation now is a triplet rather than the singlet state found in the opposite limit $E_J \gg E_C$; hence, decreasing E_J/E_C from large values, the singlet and triplet energies cross each other and the first excitation gap changes over from $3t$ (at $E_J \gg E_C$) to $2t = E_J$ (for $E_C \gg E_J$). The precise location where this crossing appears can be found from the numerical analysis described

below. The same analysis can be repeated for the connected tetrahedron; the six states degenerate under the capacitive term then involve either one or two charges on the three inner islands and the mixing term V_π describes charges hopping between the three islands as well as hopping of one charge to and from the ring.

D. Numerical Results

The above results can be verified numerically via diagonalization of the Hamiltonian (18) with the help of a Lanczos algorithm; in the charge basis the mixing term V_π then describes the hopping of charges between the islands. Going to a phase representation, the bias charges q_i are conveniently accounted for via the boundary condition for the wave function, $\Psi_n(\phi_1 + 2\pi\delta_{1k}, \phi_2 + 2\pi\delta_{2k}, \phi_3 + 2\pi\delta_{3k}) = \exp(-2\pi i q_k) \Psi_n(\phi_1, \phi_2, \phi_3)$, $k = 1, 2, 3$, after a suitable gauge transformation²². The results of such an analysis for the charge state $q_i = 1/2$ is shown in Fig. 3, where the excitation gap Δ_d protecting the qubit states against higher excitations is shown as a function of E_J/E_C . The crossover from the charge to the phase dominated regime, where the singlet and triplet excited states cross, takes place at $E_J/E_C \approx 5$. The analytic results (17) and (20) describe well the data away from the crossover regime. One expects the quasi-classic result to become exact in the limit of large E_J/E_C ; however, the result (17) has been calculated using the one-dimensional approximation V_f for the potential and one cannot expect perfect agreement with the numerical data. Still, the quasi-classic approximation turns out accurate over a very large regime extending down to parameters E_J/E_C of order 10: scaling the dashed line in Fig. 3 by 0.8 the quasi-classic result cannot be distinguished from the numerical data for $E_J/E_C > 20$.

The numerical results show that the suppression of the tunneling amplitude t is indeed small in the tetrahedron. E.g., choosing a value E_J/E_C of order 100 the energy scale t of the qubit is suppressed by a factor $\sim 2/1000$ with respect to the energy scale E_J of the junctions. For a conventional device this suppression involves an action $S \approx c\sqrt{E_J/E_C}$, with the numerical c depending on the specific setup. E.g., for the 4-junction loops studied in Ref. 24 the numerical $c \approx 1.6$ and choosing the same value of E_J/E_C this implies a suppression of quantum fluctuations by a factor $\sim \exp(-16) \sim 10^{-7}$; such a device then resides deep in the semi-classical regime and quantum effects are heavily suppressed.

In summary, we can tune our tetrahedral structure such as to realize a doubly-degenerate groundstate corresponding to a spin-1/2 system in zero magnetic field; the device can be realized using moderately large junctions with E_J/E_C of order 100 while keeping an appreciable operational energy scale t , a consequence of the particular frustration in the device. Below, we will show that this ground state remains robust to quadratic order in the external noise and hence provides a suitable starting

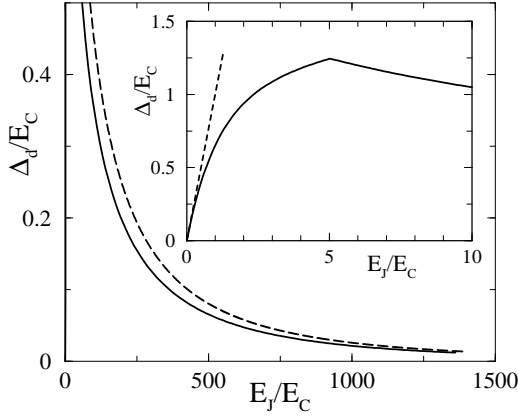


FIG. 3: Excitation gap Δ_d protecting the qubit doublet against higher excitations as a function of E_J/E_C ; the dashed line is the semi-classic result based on (17). The inset shows an expanded view illustrating the crossing of the singlet and triplet excited states as the system enters the charge dominated regime at low values of E_J/E_C ; the dashed line is the analytic result (20) valid in the charge dominated regime $E_C \gg E_J$. Data obtained with help of a Lanczos algorithm operating in the charge representation with 27 charge states between $q = \pm 13$.

point for the construction of a qubit; we will concentrate on this doubly-degenerate case and its use for quantum computing in the following.

E. External fields

Fabrication errors and external bias induce splittings and shifts in the levels. With respect to the qubit's functionality, random external signals produce decoherence, while prescribed bias signals are used for its manipulation. Fabrication errors mainly affect the coupling E_J of the junctions — we denote the corresponding deviations by $\epsilon_{ij}E_J$ (note that the fabrication tolerance is improved for larger junctions, leading to smaller values of ϵ_{ij}). External bias signals appear randomly through fluctuations in the local magnetic field and through stray charges; artificially generated signals can be applied through properly placed current loops biasing the sub-loops of the tetrahedron (currents i_i in Fig. 1) and through capacitive charging of the islands (via voltages v_i). We denote the corresponding bias fields by $\delta_i^\Phi \equiv -2\pi\Phi_i/\Phi_0$ and $\delta_i^Q \equiv \delta q_i$, $i = 1, 2, 3$. E.g., for the isolated tetrahedron the flux Φ_3 penetrating the sub-loop ‘0-1-2’ is encoded in a bias angle $\delta_3^\Phi \equiv \delta(\phi_2 - \phi_1) = -2\pi\Phi_3/\Phi_0$ along the link ‘1-2’; equivalent definitions apply to the other sub-loops with the cyclic replacement $3 \rightarrow 1 \rightarrow 2 \rightarrow 3$. For the connected tetrahedron we have to account for the total flux Φ threading the outer ring; assuming a symmetric setup, this flux will induce the phase shifts $\delta = -2\pi\Phi/3\Phi_0$ in each of the segments ‘m1-m2’, ‘m2-m3’, and ‘m3-m1’, cf. Fig. 1(b). The bias angles δ_i^Φ along

the links ‘ j - k ’ then have to account for this flux via the modified form $\delta_i^\Phi = 2\pi(\Phi_i - \Phi/3)/\Phi_0$, where Φ_i denotes the flux through the loop ‘ m - j - m - k - j - m ’. Note that we have assumed that the currents circulating in the outer ring are still sufficiently small such as not to produce significant self-fields. While the charge bias δ_i^Q only affects the tunneling matrix elements t_{ij} , i.e., the kinetic energy term, the flux bias δ_i^Φ modifies both the potential and the kinetic energy terms in the Lagrangian.

We first determine the modification of the potential energy V_π , cf. (1), due to applied fluxes δ_i^Φ ,

$$\frac{V_\pi}{2E_J} = \cos\left(\chi_1 + \frac{\delta_3^\Phi}{2}\right) \cos\left(\chi_2 - \frac{\delta_3^\Phi}{2}\right) + \cos\left(\chi_3 + \frac{\delta_2^\Phi}{2}\right) \times \cos\left(\chi_1 - \frac{\delta_2^\Phi}{2}\right) + \cos\left(\chi_2 + \frac{\delta_1^\Phi}{2}\right) \cos\left(\chi_3 - \frac{\delta_1^\Phi}{2}\right). \quad (21)$$

Assuming small perturbations, we expand (21) in $\delta_i^\Phi \ll \omega_f/E_J$; we concentrate on the point $O_2 = (0, -\pi, 0)$ and combine the result with the kinetic term to arrive at the Hamiltonian (6) with the additional term

$$\frac{\delta H}{E_J} = -\left[\delta_1^\Phi(\delta\chi_3 - \delta\chi_2) + \delta_2^\Phi(\delta\chi_3 - \delta\chi_1) + \delta_3^\Phi(\delta\chi_2 - \delta\chi_1) - \frac{1}{2}(\delta_1^{\Phi 2} + \delta_3^{\Phi 2} - \delta_2^{\Phi 2})\right]. \quad (22)$$

Classically, the force term in (22) lowers the energy indefinitely as the system runs away along the degenerate classical minimal lines; e.g., a perturbation $\delta_2^\Phi > 0$ produces a runaway either along the $(0, 0, \delta\chi_3)$ direction or along the $(-\delta\chi_1, 0, 0)$ direction. However, quantum fluctuations generate a finite potential along these lines, resulting in a linear response in the coordinates $\delta\chi_i$ and a quadratic change in energy v_2 . Indeed, second-order perturbation theory in the force term of (21) produces the result

$$\frac{v_2}{E_J} = -\nu \left[(\delta_1^\Phi + \delta_2^\Phi)^2 + (\delta_2^\Phi + \delta_3^\Phi)^2 \right] + (\epsilon_{02} - \epsilon_{03} - \epsilon_{01}) + (\epsilon_{31} - \epsilon_{12} - \epsilon_{23}), \quad (23)$$

with

$$\nu \approx 1.0 (E_J/E_C)^{1/3} \quad (24)$$

obtained from a numerical solution of the perturbed eigenvalue problem combining (6) and (22). In (23) we have dropped the term $(E_J/2)(\delta_1^{\Phi 2} + \delta_3^{\Phi 2} - \delta_2^{\Phi 2})$ as it is small by a factor $(E_C/E_J)^{1/3}$ compared to the leading term; also, we have added a term due to deviations $\epsilon_{ij}E_J$ in the junction couplings. Equivalent expressions for the other minima follow from cyclic permutation of the indices. As a result, we obtain the relative shifts $v_{ij} \equiv v_j - v_i$ ($i, j, k = 1, 2, 3, k \neq i, j$)

$$\frac{v_{ij}}{E_J} = \nu(\delta_i^\Phi - \delta_j^\Phi)(\delta_i^\Phi + \delta_j^\Phi + 2\delta_k^\Phi) + 2(\epsilon_{0j} - \epsilon_{0i} + \epsilon_{ki} - \epsilon_{jk}) \quad (25)$$

in the minima. First, we note that small random fluxes do not affect these positions in the first order of these fluctuations; the corrections appearing in quadratic order then are small. Second, we note that fabrication errors ϵ_{ij} in the junction couplings can be compensated by appropriate choices of bias fluxes δ_i^Φ .

In the determination of the perturbed tunneling matrix elements t_{ij} , we ignore the modifications arising due to fabrication errors and concentrate on the effects of flux and charge signals, random or externally applied. By way of example, we calculate the tunneling matrix elements t_{12} and t_{21} connecting the states $|O_1\rangle$ and $|O_2\rangle$. The presence of perturbing fluxes δ_1^Φ and δ_2^Φ shifts the potential V_π by v along the line γ , to lowest order in δ_i^Φ , $v(\chi) = -E_J \sin \chi (\delta_1^\Phi + \delta_2^\Phi)$. This shift produces the changes $\delta S_{12}^\pm = \mp s(\delta_1^\Phi + \delta_2^\Phi)$ (the correction δS_{12}^+ applies to the trajectory γ in Fig. 2(a)) with

$$s \approx 1.5 (E_J/E_C)^{3/4} \quad (26)$$

in the action S_f determining the modulus $|a|$ of the tunneling amplitude (10); as before, the expression (26) is valid deep in the semi-classical regime.

The presence of perturbing charges δ_1^Q and δ_2^Q modifies the Aharonov-Bohm-Casher phase associated with the two trajectories (a charge Q encircling a flux Φ counter clockwise produces the phase $\exp[2\pi i(\Phi/\Phi_0)(Q/2e)]$; they pick up the additional phases $\exp[\pm i\pi(\delta_1^Q + \delta_2^Q)]$, with the plus sign belonging to the trajectory γ , cf. Fig. 2(b). Combining the perturbations in the fluxes and charges, the change in the tunneling amplitudes $\delta t_{12} = t_{12}^s + it_{12}^a = \delta t_{21}^*$ takes the form

$$\frac{\delta t_{12}}{t} = \frac{e^{-\delta S_{12}^+ + i\pi(\delta_1^Q + \delta_2^Q)} + e^{-\delta S_{12}^- - i\pi(\delta_1^Q + \delta_2^Q)} - 2}{2}; \quad (27)$$

expanding the exponentials, the symmetric and antisymmetric parts are given by the expressions

$$\begin{aligned} t_{12}^s &= t [s^2(\delta_1^\Phi + \delta_2^\Phi)^2/2 - \pi^2(\delta_1^Q + \delta_2^Q)^2/2], \\ t_{12}^a &= \pi s t (\delta_1^\Phi + \delta_2^\Phi)(\delta_1^Q + \delta_2^Q); \end{aligned} \quad (28)$$

further terms quadratic in δ^Φ (e.g., arising from the next term in the expansion of S_f) are small by the factor $(E_C/E_J)^{1/4}$. With respect to the qubit's stability, we note that all perturbations appear in second order of the small quantities δ_i^Φ and δ_i^Q . In the further analysis below we will drop the flux bias term $\propto \delta_i^{\Phi^2}$ in t_{ij}^s against the (parametrically large) shifts v_i in the potential energy.

We determine the new energy levels perturbatively: the perturbation δH , written in the space of semi-classical ground states $|O_i\rangle$, takes the form

$$\delta H_O = \begin{pmatrix} v_1 & t_{12}^s + it_{12}^a & t_{31}^s - it_{31}^a \\ t_{12}^s - it_{12}^a & v_2 & t_{23}^s + it_{23}^a \\ t_{31}^s + it_{31}^a & t_{23}^s - it_{23}^a & v_3 \end{pmatrix}. \quad (29)$$

Next, we find the corresponding matrix elements $\langle \pm | \delta H | \pm \rangle$ in the projected space spanned by the doublet $|\pm\rangle$, cf. (15). It is convenient to cast the result of

this calculation into the form

$$H_{\text{qubit}} = e_d \mathbf{1} + \mathbf{h} \cdot \boldsymbol{\sigma} \quad (30)$$

with $\boldsymbol{\sigma} = (\sigma_x, \sigma_y, \sigma_z)$ the Pauli matrices; switching of the 'magnetic' fields h_x and h_z then produces the standard amplitude- and phase-shift operations required for the manipulation of the individual qubit. The shift e_d and the effective 'magnetic' field \mathbf{h} are given by the expressions

$$\begin{aligned} e_d &= \frac{1}{3} [v_1 + v_2 + v_3 - (t_{12}^s + t_{23}^s + t_{31}^s)], \\ h_x &= \frac{1}{3} \left[v_1 - \frac{1}{2}(v_2 + v_3) + (2t_{23}^s - t_{12}^s - t_{31}^s) \right], \\ h_y &= \frac{1}{2\sqrt{3}} (v_3 - v_2) + \frac{1}{\sqrt{3}} (t_{12}^s - t_{31}^s), \\ h_z &= -\frac{1}{\sqrt{3}} (t_{12}^a + t_{23}^a + t_{31}^a); \end{aligned} \quad (31)$$

note that the perturbations v_i in the potential come with the large amplitude E_J , while those in the kinetic energy ($t^{s,a}$) involve the smaller energy scale t of the tunneling matrix element; in (31) we keep both terms as we might choose to manipulate the qubit via changes in the charges δ^Q alone. Expressing the perturbations in terms of the flux- and charge-parameters δ_i^Φ and δ_i^Q we obtain the results

$$\begin{aligned} e_d &= -\frac{4\nu E_J}{3} (\delta_1^{\Phi^2} + \delta_2^{\Phi^2} + \delta_3^{\Phi^2} + \delta_1^\Phi \delta_2^\Phi + \delta_1^\Phi \delta_3^\Phi + \delta_2^\Phi \delta_3^\Phi) \\ &\quad + \frac{t\pi^2}{6} [(\delta_1^Q + \delta_2^Q)^2 + (\delta_2^Q + \delta_3^Q)^2 + (\delta_3^Q + \delta_1^Q)^2], \\ h_x &= \frac{\nu E_J}{6} [2(\delta_2^\Phi + \delta_3^\Phi)^2 - (\delta_1^\Phi + \delta_2^\Phi)^2 - (\delta_1^\Phi + \delta_3^\Phi)^2] \\ &\quad + \frac{t\pi^2}{6} [2\delta_1^{Q^2} - \delta_2^{Q^2} - \delta_3^{Q^2} - 2\delta_3^Q(\delta_2^Q - \delta_1^Q) \\ &\quad \quad - 2\delta_2^Q(\delta_3^Q - \delta_1^Q)], \\ h_y &= \frac{\nu E_J}{2\sqrt{3}} (2\delta_1^\Phi + \delta_2^\Phi + \delta_3^\Phi)(\delta_2^\Phi - \delta_3^\Phi) \\ &\quad + \frac{t\pi^2}{2\sqrt{3}} [\delta_3^{Q^2} - \delta_2^{Q^2} + 2\delta_1^Q(\delta_3^Q - \delta_2^Q)], \\ h_z &= -\frac{\pi s t}{\sqrt{3}} [(\delta_1^\Phi + \delta_2^\Phi)(\delta_1^Q + \delta_2^Q) \\ &\quad + (\delta_2^\Phi + \delta_3^\Phi)(\delta_2^Q + \delta_3^Q) + (\delta_3^\Phi + \delta_1^\Phi)(\delta_3^Q + \delta_1^Q)]. \end{aligned} \quad (32)$$

For convenience, we also cite the energy shift e_s of the singlet state,

$$\begin{aligned} e_s &= \frac{1}{3} [v_1 + v_2 + v_3 + 2(t_{12}^s + t_{23}^s + t_{31}^s)], \\ &= -\frac{4\nu E_J}{3} (\delta_1^{\Phi^2} + \delta_2^{\Phi^2} + \delta_3^{\Phi^2} + \delta_1^\Phi \delta_2^\Phi + \delta_1^\Phi \delta_3^\Phi + \delta_2^\Phi \delta_3^\Phi) \\ &\quad - \frac{t\pi^2}{3} [(\delta_1^Q + \delta_2^Q)^2 + (\delta_2^Q + \delta_3^Q)^2 + (\delta_3^Q + \delta_1^Q)^2]. \end{aligned} \quad (33)$$

While the bias variables δ_i^Φ and δ_i^Q as well as the fields $e_{d,s}$ and h_z do respect the symmetry of the tetrahedron, the

bias fields h_x and h_y do not. The tetrahedral symmetry may be made explicit by reexpressing the planar field \mathbf{h}_\perp in the hexagonal basis $\mathbf{e}_1 = (1, 0)$, $\mathbf{e}_2 = (-1/2, -\sqrt{3}/2)$, $\mathbf{e}_3 = (-1/2, \sqrt{3}/2)$, $\mathbf{h}_\perp = \sum_i h_i \mathbf{e}_i$ with

$$h_i = \frac{\nu E_J}{3} (\delta_j^\Phi + \delta_k^\Phi)^2 + \frac{t\pi^2}{3} [\delta_i^Q{}^2 + 2\delta_i^Q(\delta_j^Q + \delta_k^Q)^2]; \quad (34)$$

the relation between the tetrahedral symmetries and the rotations in spin space then becomes obvious. The three symmetric fields h_i relate to the two cartesian fields via $h_x = h_1 - (h_2 + h_3)/2$ and $h_y = \sqrt{3}(h_2 - h_3)/2$; there is no inverse transformation.

III. NOISE SENSITIVITY AND MANIPULATION

The above results exhibit two remarkable features of our tetrahedral qubit:

i) Both, charge and flux noise appear only to quadratic order, a feature which is easily traced back to the absence of polarization charges and currents in the qubit's ground state. This guarantees for a long decoherence time of the tetrahedral qubit, similar to the 'quantronium' discussed by Vion *et al.*⁷. Numerical analysis confirms the weak susceptibility to charge noise: a uniform random bias $V \in [-V_0, V_0]$ acting on the islands produces a small doublet splitting $\delta \approx 0.2 \Delta_d (2eV_0/EC)^2$, roughly independent of E_J/EC . At the same time, the quadratic dependence on bias allows for a qubit manipulation via *ac*-fields and the dangerous low-frequency noise can be blocked with appropriate filters.

ii) The tetrahedral qubit admits a large variety of manipulation schemes using either magnetic or electric bias. The 'planar fields' h_x and h_y can be manipulated via changes in flux alone, e.g., setting $\delta_2^\Phi = \delta_3^\Phi = \delta^\Phi \neq \delta_1^\Phi/a_x$ with $a_x = (-1 \pm 2)$, we can direct the field along the x -axis, while the flux state $\delta_1^\Phi = \delta^\Phi[(1 + a_y^2)/2]^{1/2}$, $\delta_2^\Phi/a_y = \delta_3^\Phi = \delta^\Phi$, with $a_y = -(2 + \sqrt{3})$ produces a field pointing in the y -direction (here, we assume no charge bias, $\delta_i^Q = 0$; with these choices of parameters the sub-leading term $E_J(\delta_1^{\Phi^2} + \delta_3^{\Phi^2} - \delta_2^{\Phi^2})/2$ in (22) contributing to h_x with $(E_J/6)[\delta_2^{\Phi^2} + \delta_3^{\Phi^2} - 2\delta_1^{\Phi^2}]$ and to h_y with $(E_J/2\sqrt{3})[\delta_2^{\Phi^2} - \delta_3^{\Phi^2}]$, vanish as well). Proper choice of amplitudes and phases allows for the generation of a rotating planar field. The axial field h_z , however, involves a modification of fluxes *and* charges, cf. (32); choosing a uniform flux- $\delta_i^\Phi = \delta^\Phi$ and a uniform charge-bias $\delta_i^Q = \delta^Q$ produces a pure axial field

$$h_z = -4\pi\sqrt{3}st\delta^\Phi\delta^Q. \quad (35)$$

The free manipulation of the 'magnetic field' $\mathbf{h}(t)$ allows for the implementation of Berry-phase type phenomena^{26,27,28}. E.g., the following provides a simple realization of the NOT-operator in the basis $|s, a\rangle = [|+\rangle \pm |-\rangle]/\sqrt{2}$: adiabatically rotating the transverse

components $h_{x,y} = h_\perp \exp(i\omega_{h_\perp} t)$, while keeping the z -component h_z fixed, defines the operator $\hat{U}_{\text{Berry}} = \exp(i\sigma_z \Omega/2)$ after one period of rotation. Here, $\Omega = 2\pi(1 - h_z/\sqrt{h_z^2 + h_\perp^2})$ is the solid angle spanned by the rotating field-cone. Selecting a field vector \mathbf{h} pointing at an angle of 60° with respect to the z -axis, the resulting operator $\exp(i\pi\sigma_z/2)$ changes the relative sign of the components along $|\pm\rangle$, i.e., the eigenstates $|s, a\rangle$ of the operator σ_x transform into one another upon each period of field rotation. Note that operator \hat{U}_{Berry} does not depend upon the rotating field frequency ω_{h_\perp} as long as $\omega_{h_\perp}^{-1}$ is much shorter than the qubit's decoherence time t_{dec} .

IV. MEASUREMENTS

Finally, we discuss several potential procedures for the measurement of our qubit's state. We assume an ideal symmetric device. As the qubit reacts to external bias only in second order, the measurement of its state involves a two-step process: In a first step, the qubit is pushed away from the symmetric point of operation through appropriate driving via external charge (δ_i^Q) and flux (δ_i^Φ) bias. As a consequence, the previously quiet qubit state now develops finite internal currents and polarization charges. In a second step, these signals have to be measured by appropriate devices and the meter reading will tell about the qubit's state.

As a simple illustration we consider the measurement of the qubit's state in the basis $|\pm\rangle$, i.e., the operator σ_z , using a charge bias $\delta_i^Q \ll 1$. This charge bias generates a current flow within the qubit and the associated flux can be measured by an external SQUID loop²⁹, cf. Fig. 4(a). We express the matrix (29) in the basis $\{|+\rangle, |-\rangle, |0\rangle\}$,

$$\delta H_O = \begin{pmatrix} e_d + h_z & h_x - ih_y & e_0^+ + ih_{0y}^+ \\ h_x + ih_y & e_d - h_z & e_0^- - ih_{0y}^- \\ e_0^+ - ih_{0y}^+ & e_0^- + ih_{0y}^- & e_s \end{pmatrix}, \quad (36)$$

with $e_{d,s}$, h_x, h_y, h_z given in (31) and (33) above and

$$\begin{aligned} e_0^\pm &= \frac{1}{6}[2v_1 - v_2 - v_3 - (2t_{23}^s - t_{12}^s - t_{31}^s)] \\ &\quad \pm \frac{1}{2\sqrt{3}}(2t_{23}^a - t_{12}^a - t_{31}^a), \\ h_{0y}^\pm &= \frac{1}{2\sqrt{3}}[v_3 - v_2 - (t_{12}^s - t_{31}^s)] \pm \frac{1}{2}(t_{12}^a - t_{31}^a). \end{aligned} \quad (37)$$

A finite 'magnetic field' $\mathbf{h} = (0, 0, h_z)$ induces the shifts $\delta E^\pm = \pm h_z$ in the two states $|\pm\rangle$. Charge-biasing the device induces the current (we assume $\delta_i^Q \ll 1$)

$$\begin{aligned} I_i^\pm &= \frac{2e}{\hbar} \frac{\partial \delta E^\pm}{\partial \delta_i^\Phi} \\ &= \mp \frac{2\pi est}{\sqrt{3}\hbar} (2\delta_i^Q + \delta_j^Q + \delta_k^Q) \end{aligned} \quad (38)$$

in the corresponding sub-loop ‘0 – j – k’ (the above signs apply to the isolated tetrahedron and have to be reversed for the connected device; a positive current runs counter clockwise around the loop). Alternatively, applying a (small) external flux-bias induces the voltage (see Fig. 4(b))

$$\begin{aligned} V_i^\pm &= \frac{1}{2e} \frac{\partial \delta E^\pm}{\partial \delta_i^\pm} \\ &= \mp \frac{\pi s t}{2e\sqrt{3}} (2\delta_i^\pm + \delta_j^\pm + \delta_k^\pm) \end{aligned} \quad (39)$$

on the island ‘i’ which can be measured via a single electron transistor (SET) device³⁰; here $i, j, k \in \{1, 2, 3\}$ and pairwise different. Choosing the bias in the ratio $\delta_i^{\Phi, Q} : \delta_j^{\Phi, Q} : \delta_k^{\Phi, Q} = 3 : -1 : -1$ limits the current/voltage to the loop/island ‘i’.

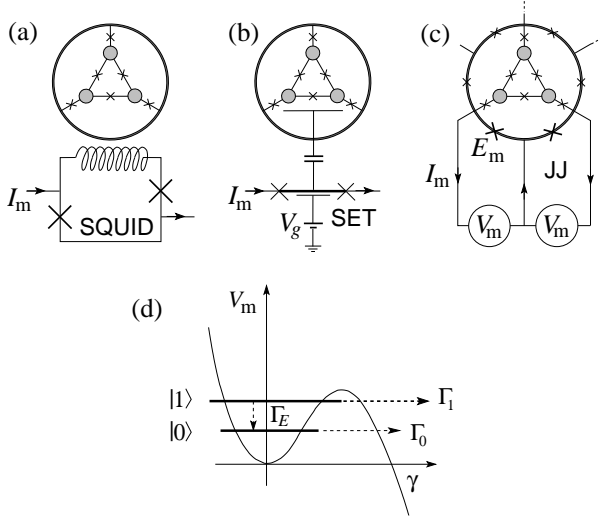


FIG. 4: Measurement setups allowing the identification of the qubit state. (a) An external charge bias induces currents in the qubit structure with a circularity depending on the qubit state. The flux associated with these currents is inductively coupled to a SQUID which is driven close to criticality during the measurement. Depending on the qubit flux, the SQUID is driven overcritical and the associated voltage is measured. (b) An external current bias induces polarization charges in the qubit structure with a polarity depending on the qubit state. The associated charge is capacitively coupled to a SET which is driven close to (charge) frustration during the measurement. Depending on the qubit’s polarization charge the SET is driven into the conducting state and the associated current is measured. (c) Similar to (a), but with qubit currents directly channelled through the measurement junctions with large couplings $E_m \gg E_J$; again, the presence of a voltage V_m in the external loop carries the information on the qubit state. (d) States of the measurement junctions (with phase γ) at fixed classical driving current I_m with a slowly decaying state $|0\rangle$ (decay rate Γ_0) and a fast decaying state $|1\rangle$ (decay rate $\Gamma_1 \gg \Gamma_0$) depending on the qubit state. We assume a slow energy relaxation for the qubit, $E_E \ll \Gamma_1$.

Several issues have to be considered in the measurement process, cf. the discussion in Ref. 31. Relevant pa-

rameters are the dephasing- and mixing rates Γ_φ and Γ_E induced by the measurement apparatus and their relation to the separation E_{01} between the qubit eigenstates; in a weak measurement scheme we have $\Gamma_\varphi \ll E_{01}$, while a projective measurement is characterized by a strong coupling with $E_{01} \ll \Gamma_\varphi$ such that the quantum evolution of the system is quenched rapidly. While dephasing transforms a coherent superposition of states into a classical mixture through elimination of the off-diagonal elements in the qubit’s density matrix, the mixing induces transitions between the qubit’s states and thus spoils the measurement. Usually, a good measurement setup makes use of decoherence in transferring classical information to the measurement device but avoids mixing, hence $\Gamma_\varphi \gg \Gamma_E$.

The simplest situation is realized when the measured observable commutes with the qubit Hamiltonian — in this case the measurement preserves the qubit’s eigenstates. On the other hand, if the measured observable does not commute with the qubit Hamiltonian, the measurement has to be completed before mixing sets in; hence $\Gamma_E < \Gamma_{\text{meas}} < \Gamma_\varphi \ll E_{01}/\hbar$ for a weak measurement, while the sequence $\Gamma_E < \Gamma_{\text{meas}} < E_{01}/\hbar \ll \Gamma_\varphi$ applies to the projective measurement (here, $\Gamma_{\text{meas}} = 1/t_{\text{meas}}$ denotes the inverse measuring time).

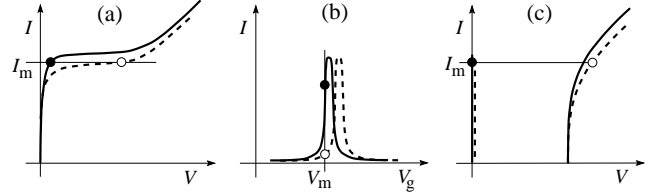


FIG. 5: Current-voltage characteristics of meter devices. The solid/dashed lines refer to the different quantum states of the qubit shifting the characteristic of the meter device. (a) In an overdamped SQUID the current-voltage characteristic is single valued, with a voltage due to a finite rate of individual phase-slips. I_m is the imposed measuring current. (b) The current in the SET results from a continuous flow of individual electrons traversing the island. V_m is the imposed gate voltage during measurement. (c) An underdamped SQUID/Josephson junction exploits an instability where a single phase-slip triggers a transition to the dissipative branch.

The measurement schemes described in Ref. 31 involve dissipative meter devices, e.g., an overdamped SQUID with a well defined (single-valued) current-voltage characteristic as depicted in Fig. 5(a) or a SET with the characteristic shown in Fig. 5(b). In both cases the measurement involves numerous dissipative events, either many phase-slips producing the voltage across the SQUID device or many electrons traversing the island of the SET. The fluctuations due to the phase slips/electrons act back on the qubit, enforcing its loss of phase coherence. Such measurement schemes can be implemented in terms of weak or strong (projective) measurements.

This type of measurement has to be contrasted with a meter characterized by an instability, such as an un-

derdamped SQUID or Josephson junction with a characteristic as shown in Fig. 5(c). Such a meter does not couple dissipatively to the qubit but switches to a dissipative state only after the measurement, e.g., after the occurrence of one phase slip, hence $\Gamma_\varphi \ll E_{01}$; the measurement is weak and generates a small imaginary part to the energy of the qubit eigenstate which then may be determined in a decay process. The qubit states are identified through their (exponentially) different decay rates. Such a measurement scheme has been used recently by Vion *et al.*⁷. In their setup, an additional measurement junction is introduced into the qubit loop. The current generated by the qubit is superimposed on an external measurement current and drives the measurement junction towards criticality, see Fig. 4(c). Here, we make use of the symmetric setup shown in Fig. 6(a) involving six classical measurement junctions with equal couplings $E_m \gg E_J$. The measuring currents I_{mi} are fed into the device through the points ‘n1’, ‘n2’, and ‘n3’ and removed at the points ‘m1’, ‘m2’, and ‘m3’. The measuring current I_m flowing in the segments ‘n3-m1’ and ‘n3-m2’ (and in the other obtained through cyclic permutation) is chosen close to the critical current $I_{m,c} = 2eE_m/\hbar$ of the measurement junctions, requiring to feed a current $I_{\text{ext}} \approx 2I_{m,c}$ into the tetrahedron via the input lines ‘n1’, ‘n2’, ‘n3’ and retraining them via the output lines ‘m1’, ‘m2’, ‘m3’. A convenient measuring setup is the symmetric one with equal currents crossing the junctions ‘n3-m1’ and ‘n3-m2’ (and other pairs obtained through cyclic permutation). Driving the qubit with external bias fields δ_l^P and δ_l^Q induces additional currents $I_{q,i}$ in the loops ‘mj-mk-k-j-mj’ which are characteristic for the quantum state of the qubit. Depending on the relative flow direction of the qubit currents and the measuring current, the six measuring junctions are either driven towards ($I_m + I_{q,i} \sim I_{m,c}$) or away ($I_m + I_{q,i} < I_{m,c}$) from criticality. The voltage pattern appearing on the six junctions then allows for the identification of the qubit state. Within this scheme, care has to be taken not to spoil the symmetry of the measurement setup by a circular current flowing in the outer ring, hence the system should be flux biased such that the total flux Φ through the ring remains zero. This can be easily achieved by compensating the fluxes Φ_i in the loops ‘mj-mk-k-j-mj’ through an equal and opposite flux $\Phi_\Delta = -\sum_{i=1}^3 \Phi_i$ through the central triangular loop.

Below, we study two schemes, a weak measurement in the Hamiltonian basis with $\Gamma_\varphi < E_{01}$ and a projective measurement onto the current basis with $E_{01} < \Gamma_\varphi$. In both cases we discuss the measurement of two operators, the measurement of σ_z and of σ_x .

A. Measurements in the qubit’s eigenbasis

A proper measurement in the energy eigenbasis imposes a number of constraints on the measuring device. First of all, the phase decoherence rate has to be small,

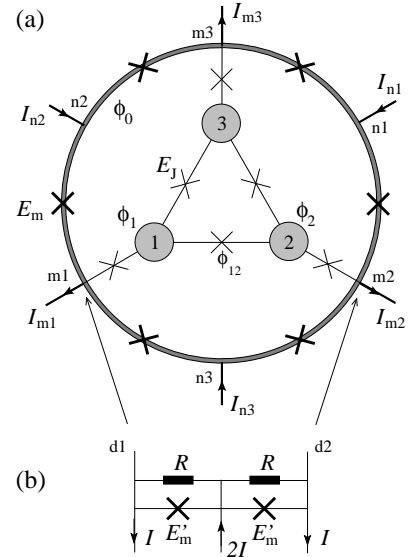


FIG. 6: (a) Symmetric setup measuring the quantum state of the qubit. Currents below twice the critical current $I_{m,c} = 2eE_m/\hbar$ of the six equal measurement junctions are fed into the qubit loop through the points ‘n1’, ‘n2’, and ‘n3’, and removed through the leads at ‘m1’, ‘m2’, and ‘m3’. The qubit current I_q flowing in the segments ‘n3-m1’ and ‘n3-m2’ (and cyclically permuted) add to these measurement currents and drive the junction towards or away from criticality. The voltage pattern measured on the six junctions tells about the qubit’s state. Care has to be taken not to spoil the symmetry in this measurement setup through a ring current in the outer loop; such a current can be avoided by appropriate compensation of the flux bias through the individual loops ‘mj-mk-k-j-mj’ with an equal and opposite flux through the central loop ‘1-2-3-1’. This can be realized, e.g., via an independent control on the individual loops and on the overall flux penetrating the entire structure. (b) circuitry introducing damping on the six measuring junctions. Driving the parallel junctions (with couplings E'_j) overcritical via a large current $2I$ switches the parallel channel into the resistive state. The contacts ‘d1’ and ‘d2’ of such a dissipative element are then connected to the points ‘m1’, ‘m2’, and ‘m3’ of the qubit structure in order to make the associated currents classical.

$\Gamma_\varphi \ll E_{01}$. The decay rate Γ_1 via tunneling of the high energy state (low barrier state, cf. Fig. 4(d)) should be large, $\Gamma_1 \gg \Gamma_E$ such that the system tunnels before decaying to the (metastable) ground state. Finally, the measurement time t_{meas} should be larger than the inverse tunneling rate, $t_{\text{meas}} > \Gamma_1^{-1}$. Note, that phase decoherence before tunneling, i.e., $\Gamma_\varphi > \Gamma_1$, is not a necessary requirement in this type of measurement; the decay may as well proceed out of the coherent state, i.e., a superposition of the qubit states. In this case, the first phase slip triggers the projection, while the subsequent phase-slips produce the large voltage signal.

In order to measure the operator σ_n , i.e., the spin projection onto the axis \mathbf{n} , we first apply a ‘magnetic field’ $\mathbf{h} = \hbar\mathbf{n}$ directed along \mathbf{n} . This is achieved via proper

charge- and flux-biasing as described by the equations (32). The doublet space $\{|+\rangle, |-\rangle\}$ then is split with new qubit eigenstates $|+\rangle_{\mathbf{n}}$ and $|-\rangle_{\mathbf{n}}$ separated by the ‘Zeeman’ energy $\Delta E = 2h$. The currents $I^{(nj-mk)}$ flowing in the segments ‘mj-nk’ across the measuring junctions are equal to the loop currents $I_{q,i}$ in ‘mj-mk-k-j-mj’ and thus are determined by the derivatives

$$I^{(nj-mk)} = I_{q,i} = -\frac{2e}{\hbar} \frac{\partial h}{\partial \delta_i^\Phi}. \quad (40)$$

In order to avoid the flow of a circular current in the outer ring, the driving flux bias δ_i^Φ has to be properly compensated as described above.

We proceed with the evaluation of the currents (40) associated with the measurement of σ_z and σ_y and generated by the application of magnetic fields h_z and h_x along the z - and x -axis, respectively. Starting with the measurement of σ_z , the projection along the z -axis, we choose a uniform charge and flux bias ($\rightarrow \mathbf{h} = (0, 0, h_z)$, cf. (32)) and obtain the qubit loop currents

$$I_{q,i}^z = \pm \frac{8\pi est}{\sqrt{3}\hbar} \delta^Q, \quad (41)$$

$i = 1, 2, 3$, in the qubit state $|\pm\rangle_z$. Hence all loops are equally driven and voltage signals on the triple ‘n1-m3’, ‘n2-m1’, ‘n3-m2’ identify the qubit state $|+\rangle$, while finite voltages on the junctions ‘n1-m2’, ‘n2-m3’, ‘n3-m1’ are associated with the $|-\rangle$ state, provided that $\delta^Q > 0$.

Second, the projection along the x -axis can be measured by applying a ‘field’ along h_x using a flux bias $\delta_2^\Phi = \delta_3^\Phi = -\delta_1^\Phi \equiv \delta^\Phi$. This bias generates a field $h_x = 4\nu E_J (\delta^\Phi)^2 / 3$ and imprints qubit currents of magnitude

$$I_{q,i}^x = \mp \frac{8e\nu E_J}{3\hbar} \delta^\Phi \quad (42)$$

for $i = 2, 3$ in the qubit state $|\pm\rangle_x$, while $I_{q,1}^x = 0$. Hence the pairs ‘n2-m1’, ‘n3-m2’, and ‘n2-m3’, ‘n3-m1’ are equal and oppositely driven, while the junctions ‘n1-m2’ and ‘n1-m3’ do not experience any additional drive due to the qubit structure.

B. Projective measurement in the current basis

A projective measurement in the current basis requires to switch on a strong decoherence $\Gamma_\varphi \gg E_{01}$ during the measurement. This decoherence then projects the state of the qubit at onset of dissipation onto the current basis and keeps it there via the Zeno (watchdog) effect, cf. Ref. 31. A suitable circuit allowing to turn on decoherence is shown in Fig. 6(b). The admittance between the points ‘d1’ and ‘d2’ is given by the expression $Z^{-1}(\omega) = 1/2R - E'_m/2i\hbar\omega R_Q$, with $R_Q = \hbar/4e^2$ the quantum resistance. Choosing parameters $R \lesssim R_Q$ (this guarantees a sufficient decoherence in the ‘on’ state, see below), $E'_m \sim (10 - 100)E_J$, and an operating frequency

$\omega \lesssim 0.1E_J$, we find that $Z \approx -2iR_Q(\hbar\omega/E'_m)$. Hence, at zero applied current I the conductance between the points ‘d1’ and ‘d2’ is dominated by the Josephson junctions and is mostly imaginary at low frequencies, allowing us to ignore dissipation (‘off’ state). However, when the system is biased by a current I larger than critical, the Josephson current disappears and the resistance R provides a significant source of dissipation as quantified through the dimensionless parameter $\alpha = R_Q/R$. In addition, while the Josephson junction itself involves a large quasi-particle resistance at low temperatures, when driven with a large current the junction switches to the resistive state with the resistance R'_m ; the latter is related to E'_m via the Ambegaokar-Baratoff relation $R'_m/R_Q = \Delta/E'_m$. The projective measurement in the current basis then starts with switching on a strong dissipation (such that $\Gamma_\varphi \gg E_{01}$) which is diagonal in the eigenbasis of the qubit’s current operator \hat{I}_q .

Before continuing with the discussion of an appropriate projective measurement in the current basis, we discuss one more issue related to the quality of such a measurement. The above measurement schemes (via coupling to a SQUID or a SET) are diagonal in the qubit’s subspace spanned by $|+\rangle$ and $|-\rangle$ and can be implemented in terms of weak and strong (projective) measurements, cf. Ref. 31. However, extending the analysis to the low-energy subspace $\{|+\rangle, |-\rangle, |0\rangle\}$, we find for the current operator $\hat{I}_1 = (2e/\hbar)\partial\delta H_O/\partial\delta_1^\Phi|_{\delta_1^\Phi=0}$ the expression (cf. (36))

$$\frac{2\pi est}{\hbar\sqrt{3}} \begin{pmatrix} -(\delta_{12}^Q + \delta_{31}^Q) & 0 & \delta_{12}^Q\zeta + \delta_{31}^Q\zeta^* \\ 0 & \delta_{12}^Q + \delta_{31}^Q & -\delta_{12}^Q\zeta^* - \delta_{31}^Q\zeta \\ \delta_{12}^Q\zeta^* + \delta_{31}^Q\zeta & -\delta_{12}^Q\zeta - \delta_{31}^Q\zeta^* & 0 \end{pmatrix},$$

where $\delta_{ij}^Q = \delta_i^Q + \delta_j^Q$; choosing a charge-bias $\delta_1^Q/3 = \delta^Q = -\delta_2^Q = -\delta_3^Q$ this reduces to

$$\hat{I}_1 = -\frac{4\pi est}{\hbar\sqrt{3}} \delta^Q \begin{pmatrix} 2 & 0 & 1 \\ 0 & -2 & -1 \\ 1 & -1 & 0 \end{pmatrix}. \quad (43)$$

Similar expressions apply to the other current operators \hat{I}_2 and \hat{I}_3 and, replacing $2\pi est/\hbar\sqrt{3} \rightarrow \pi st/2e\sqrt{3}$ in the prefactor and substituting $\delta_{ij}^Q \rightarrow \delta_{ij}^\Phi = \delta_i^\Phi + \delta_j^\Phi$, to the voltage operators $\hat{V}_i = (1/2e)\partial\delta H_O/\partial\delta_i^Q$.

Hence a projective measurement onto the current basis is in fact non-ideal as the measured observable, the current, does not commute with the Hamiltonian when going beyond the qubit sector. In a ‘high quality’ measurement of our qubit state one would request that the off-diagonal matrix elements (between the doublet and singlet states) of the operator are much smaller than the matrix elements in the doublet subspace. Otherwise, the measurement has to be repeated many times in order to arrive at a proper readout of the qubit state. We then need to identify special measurement configurations where the off-diagonal matrix elements remain small or even vanish altogether.

We will now give a specific example how this goal can be achieved for a projective measurement of the σ_z operator. We will show that a charge-bias with

$$\delta_2^Q = -\delta_3^Q = \delta^Q, \quad \delta_1^Q = 0 \quad (44)$$

results in a high-quality measurement of σ_z and σ_y if we choose a large bias $\delta^Q = 1/2$. This bias induces a current flow of equal magnitude but different chirality in the loops (cf. Fig. 6(a)) ‘m1-1-3-m3-m1’ (current I_2) and ‘m2-2-1-m1-m2’ (current I_3 ; loop currents circulating counter clockwise are positive); no current is induced in the loop ‘m3-3-2-m2-m3’. The total current through the link ‘m1-1’ is given by $I^{(m1-1)} = I_2 - I_3$ and will be used to drive the measurement current I_m fed symmetrically into the tetrahedron at the points ‘ni’ overcritical. We first describe the setup projecting the link current $I^{(m1-1)}$ and subsequently derive an explicit expression for the current operator. In a third step, we then describe the actual measurement process in detail.

We will show below that the link current $I^{(m1-1)}$ will not mix to the third state $|0\rangle$. However, this property is not shared by the individual loop currents I_2 and I_3 . It is then important to devise a setup projecting the state onto the link current $I^{(m1-1)}$ rather than the loop currents I_2 or I_3 . This is achieved by the symmetric coupling of three ‘dissipators’ in between the points ‘m1-m2’, ‘m2-m3’, and ‘m3-m1’. Turning on one of these dissipators renders the current in the corresponding link classical. In our setup we wish both loop current, I_2 and I_3 , to be classical and hence switch on the dissipators ‘m1-m2’ and ‘m1-m3’. In this situation it is the link current $I^{(m1-1)}$ which is coupled to the dissipative reservoir (the segment ‘m2-m3’ remains quantum and can be contracted to a point, cf. Fig. 7) and hence the quantum state is projected to a state with fixed current $I^{(m1-1)}$. In an ideally symmetric setup this current will be symmetrically split into the two arms ‘m1-m2’ and ‘m1-m3’ and, depending on the qubit state, will drive a specific set of junctions overcritical.

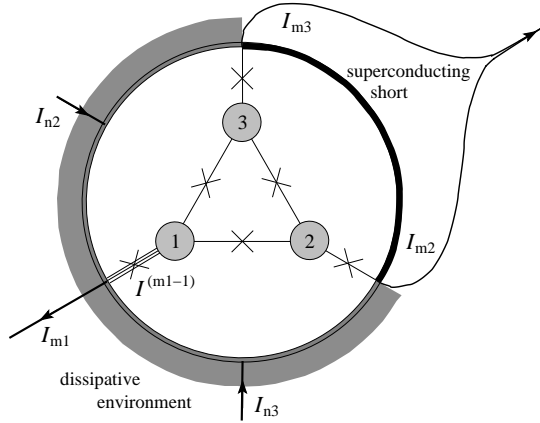


FIG. 7: Dissipative measurement setup projecting the qubit state onto the fixed link current $I^{(m1-1)}$.

Let us then turn to the calculation of the link current $I^{(m1-1)}$. In a first step, we have to generalize the tunneling

matrix elements (28) to allow for a large charge bias,

$$\begin{aligned} t + t_{ij}^s &= t \cos(\pi\delta_{ij}^Q), \\ t_{ij}^a &= st \delta_{ij}^Q \sin(\pi\delta_{ij}^Q). \end{aligned} \quad (45)$$

Assuming the above form of charge bias, the Hamiltonian in the basis of semi-classical states $\{|O_1\rangle, |O_2\rangle, |O_3\rangle\}$ takes the form $H_O = th_{Or} + isth_{Oi}$ with

$$h_{Or} = \begin{pmatrix} 0 & \cos(\pi\delta^Q) & \cos(\pi\delta^Q) \\ \cos(\pi\delta^Q) & 0 & 1 \\ \cos(\pi\delta^Q) & 1 & 0 \end{pmatrix} \quad (46)$$

and

$$h_{Oi} = \begin{pmatrix} 0 & \delta_{12}^* \sin(\pi\delta^Q) & \delta_{31}^* \sin(\pi\delta^Q) \\ -\delta_{12}^* \sin(\pi\delta^Q) & 0 & 0 \\ -\delta_{31}^* \sin(\pi\delta^Q) & 0 & 0 \end{pmatrix}, \quad (47)$$

where $\delta_{ij}^* = \delta_i^* + \delta_j^*$. The link current operator then takes the form (after setting $\delta_{ij}^* = 0$; note the sign change for the connected tetrahedron, $\hat{I}_i = -(2e/\hbar)\partial\delta H_O/\partial\delta_i^*$)

$$\hat{I}^{(m1-1)} = \frac{2est}{\hbar} \sin(\pi\delta^Q) \begin{pmatrix} 0 & -1 & 1 \\ 1 & 0 & 0 \\ -1 & 0 & 0 \end{pmatrix}. \quad (48)$$

In measuring the qubit’s state, we first drive the tetrahedron adiabatically towards the measuring point $\delta^Q = 1/2$. At small values of $\delta = (\pi\delta^Q)^2/2$ the doublet splits and we find the new eigenvalues E_δ and associated eigenvectors $|e_\delta\rangle$ (up to normalization),

$$\begin{aligned} E_\delta/t & & |e_\delta\rangle \\ -1 & & |a_\delta\rangle = i \frac{|O_2\rangle - |O_3\rangle}{\sqrt{2}}, \\ -1 + \frac{4\delta}{3} & & |s_\delta\rangle \approx \frac{2(1+\delta/3)|O_1\rangle - |O_2\rangle - |O_3\rangle}{\sqrt{6+8\delta/3}}, \\ 2 - \frac{4\delta}{3} & & |0_\delta\rangle \approx \frac{(1-\delta/3)|O_1\rangle + |O_2\rangle + |O_3\rangle}{\sqrt{3-2\delta/3}}. \end{aligned} \quad (49)$$

Note that at $\delta = 0$ the eigenvectors $|a_0\rangle$ and $|s_0\rangle$ defining the low-energy qubit subspace correspond to the (anti-) symmetric combinations $|a_0\rangle = [|+\rangle - |-\rangle]/\sqrt{2}$ and $|s_0\rangle = [|+\rangle + |-\rangle]/\sqrt{2}$. Hence starting with a qubit state $|\Psi\rangle = \psi_+|+\rangle + \psi_-|-\rangle$ in the σ_z basis $|\pm\rangle$, the amplitudes which evolve adiabatically towards the measurement point are the combinations $\psi_{s_0} = (\psi_+ + \psi_-)/\sqrt{2}$ and $\psi_{a_0} = (\psi_+ - \psi_-)/\sqrt{2}$ or, in matrix form,

$$\begin{pmatrix} \psi_{a_0} \\ \psi_{s_0} \\ \psi_{0_0} \end{pmatrix} = \hat{T} \begin{pmatrix} \psi_+ \\ \psi_- \\ \psi_0 \end{pmatrix} = \frac{1}{\sqrt{2}} \begin{pmatrix} 1 & -1 & 0 \\ 1 & 1 & 0 \\ 0 & 0 & 1 \end{pmatrix} \begin{pmatrix} \psi_+ \\ \psi_- \\ \psi_0 \end{pmatrix}.$$

Driving the bias up to $\delta^Q = 1/2$ the spectrum and eigen-

vectors deform into

$$\begin{array}{ll} E_{1/2}/t & |e_{1/2}\rangle \\ -1 & |a_{1/2}\rangle = i[|O_2\rangle - |O_3\rangle]/\sqrt{2}, \\ 0 & |s_{1/2}\rangle = |O_1\rangle, \\ 1 & |0_{1/2}\rangle = [|O_2\rangle + |O_3\rangle]/\sqrt{2}. \end{array} \quad (50)$$

In this new basis $\{|a_{1/2}\rangle, |s_{1/2}\rangle, |0_{1/2}\rangle\}$ the current operator (48) takes the form

$$\hat{I}^{(m1-1)} = \frac{2\sqrt{2}est}{\hbar} \begin{pmatrix} 0 & 1 & 0 \\ 1 & 0 & 0 \\ 0 & 0 & 0 \end{pmatrix}; \quad (51)$$

hence after the adiabatic evolution, the current measures the σ_x operator in the basis (50) and has no matrix elements with the third state $|0_{1/2}\rangle$. At the same time, the qubit wave function takes the form $|\Psi\rangle = e^{-i\theta/2}\psi_{a0}|a_{1/2}\rangle + e^{i\theta/2}\psi_{s0}|s_{1/2}\rangle$, where $\theta = \int dt(E_a - E_s)/\hbar$ denotes the additional phase picked up in the adiabatic evolution of the qubit amplitudes $\psi_{s\delta}$ and $\psi_{a\delta}$ until the measurement is performed. In order to reexpress the current (51) through the original qubit amplitudes Ψ_{\pm} we define the matrix

$$\hat{T}_{\theta} = \frac{1}{\sqrt{2}} \begin{pmatrix} e^{-i\theta/2} & -e^{-i\theta/2} & 0 \\ e^{i\theta/2} & e^{i\theta/2} & 0 \\ 0 & 0 & 1 \end{pmatrix}$$

and find the result

$$\hat{T}_{\theta}^{\dagger} \hat{I}^{(m1-1)} \hat{T}_{\theta} = \frac{2\sqrt{2}est}{\hbar} \begin{pmatrix} \cos\theta & i\sin\theta & 0 \\ -i\sin\theta & -\cos\theta & 0 \\ 0 & 0 & 0 \end{pmatrix} \quad (52)$$

describing a high quality measurement of the qubit operators $\pm\sigma_z$ at $\theta = n\pi$ and $\pm\sigma_y$ at $\theta = (n + 1/2)\pi$ (or any component residing in the y - z plane for angles θ in between). Applying the charge bias (44) to cyclically permuted islands $1 \rightarrow 2 \rightarrow 3 \rightarrow 1$ produces measurements of spin-projections in planes rotated by the corresponding angles $\pm 2\pi/3$.

In the following, we restrict the discussion to the measurement of σ_z , i.e., we assume that $\theta = n\pi$ with n even in the specific discussion below. Following the result (52), the link current $I^{(m1-1)}$ has opposite signs for the two qubit-states $|+\rangle$ and $|-\rangle$ and its measurement allows for the determination of the qubit's final wave function. In the actual measurement, the system is driven symmetrically with equal external currents $I_{ni} = I_m$ entering the system at the points 'n1', 'n2', 'n3' (cf. Fig. 6(a)) and leaving symmetrically through the points 'm1', 'm2', and 'm3'. The external current I_m is chosen close to, but below twice the critical current of the large junctions in the ring, $I_{m1} < 2I_{mc} = 4eE_m/\hbar$. Accounting for the additional currents induced in the tetrahedron under the charge bias $\delta^Q = 1/2$, the currents $I^{(n2-m1)}$

and $I^{(n3-m1)}$ through the large measurement junctions are equal to $(I_m \pm 2\sqrt{2}est/\hbar)/2$ for the $|\pm\rangle$ states of the doublet, while the currents $I^{(n2-m3)}$ and $I^{(n3-m2)}$ assume the values $(I_m \mp 2\sqrt{2}est/\hbar)/2$ for the same eigenstates. Note that in the singlet state the bare measurement current $I_m/2$ flows through the junctions as no current is induced in the singlet state $|0\rangle$ under the above charge bias. As demonstrated in Ref. 7, the measurement current I_m and the induced current $2\sqrt{2}est/\hbar$ can be chosen such that the switching probabilities \mathcal{P}_{\pm} into the transient voltage-state of the large measurement junctions are strongly different for the $|\pm\rangle$ states. Then the location of voltage pulses on the junctions 'n2-m1' and 'n3-m1' or on the complementary junctions 'n2-m3' and 'n3-m2' tells us whether the qubit was in the $|+\rangle$ or $|-\rangle$ state just before the measurement. Furthermore, the absence of any voltage pulse is the signature of the singlet state.

Finally, we discuss the projective measurement of the operator σ_x . Following (32), a flux bias produces finite 'magnetic fields' $h_{x,y}$ which are bilinear in δ_j^{Φ} ; one then may expect that an appropriate flux bias will produce loop currents which are diagonal in the basis $|a, s\rangle$, where

$$|a\rangle = (|+\rangle - |-\rangle)/\sqrt{2}, \quad |s\rangle = (|+\rangle + |-\rangle)/\sqrt{2}. \quad (53)$$

Here, we concentrate on the main contribution (proportional to ν) originating from the modification v_j in the energies of the semi-classical minima $|O_j\rangle$. The current operators $\hat{I}_i = -(2e/\hbar)\partial\delta H_O/\partial\delta_i^{\Phi}$ evaluated in the basis $\{|+\rangle, |-\rangle, |0\rangle\}$ take the form

$$\hat{I}_i = \frac{2e\nu E_J}{3\hbar} \begin{pmatrix} \epsilon_i & \lambda_i & \lambda_i^* \\ \lambda_i^* & \epsilon_i & \lambda_i \\ \lambda_i & \lambda_i^* & \epsilon_i \end{pmatrix} \quad (54)$$

with $\epsilon_i = 4(2\delta_i^{\Phi} + \delta_j^{\Phi} + \delta_k^{\Phi})$ and

$$\begin{aligned} \lambda_1 &= (2\delta_1^{\Phi} + \delta_2^{\Phi} + \delta_3^{\Phi}) + i\sqrt{3}(\delta_2^{\Phi} - \delta_3^{\Phi}), \\ \lambda_2 &= -(2\delta_3^{\Phi} + \delta_2^{\Phi} - \delta_1^{\Phi}) + i\sqrt{3}(\delta_1^{\Phi} + \delta_2^{\Phi}), \\ \lambda_3 &= -(2\delta_2^{\Phi} + \delta_3^{\Phi} - \delta_1^{\Phi}) - i\sqrt{3}(\delta_1^{\Phi} + \delta_3^{\Phi}). \end{aligned} \quad (55)$$

Applying a specific bias $\delta_2^{\Phi} = \delta_3^{\Phi} = -\delta_1^{\Phi} = \delta^{\Phi}$ produces a field along h_x (cf. (32)) and induces the current $I^{(m3-3)} \equiv I_1 - I_2 = -I^{(m2-2)}$ in the loop 'm1-m3-3-1-2-m2-m1',

$$\hat{I}^{(m3-3)} = -\frac{8e\nu E_J \delta^{\Phi}}{3\hbar} \begin{pmatrix} 2 & -1 & -1 \\ -1 & 2 & -1 \\ -1 & -1 & 2 \end{pmatrix}; \quad (56)$$

the current operator $\hat{I}^{(m1-1)}$ vanishes. Transforming to the basis states $|a, s\rangle$ of σ_x , this takes the form

$$\hat{I}^{(m3-3)} = -\frac{8e\nu E_J \delta^{\Phi}}{3\hbar} \begin{pmatrix} 3 & 0 & 0 \\ 0 & 1 & -\sqrt{2} \\ 0 & -\sqrt{2} & 2 \end{pmatrix}; \quad (57)$$

obviously, the anti-symmetric state $|a\rangle$ is already a good eigenstate of the current operator, while the states $|s\rangle$

and $|0\rangle$ remain mixed. Diagonalizing, we find the eigenvalues $-8e\nu\delta^*j/\hbar$ and eigenvectors $|j\rangle$,

$$\begin{array}{cc} j & |j\rangle \\ 1 & |a\rangle, \\ 1 & [|s\rangle - \sqrt{2}|0\rangle]/\sqrt{3}, \\ 0 & [\sqrt{2}|s\rangle + |0\rangle]/\sqrt{3}. \end{array} \quad (58)$$

The diagonal structure of $\hat{I}^{(m3-3)}$ in the subspace spanned by $|a\rangle$ and $|s\rangle$ implies a measurement of the spin-component σ_x in the original basis $|\pm\rangle$. Unfortunately, we have not been able to identify a setup producing a complete diagonalization of the current operator; still, the above constellation allows for a well defined statistical procedure to identify the qubit state: Let us assume that just before the measurement the wave function of the qubit belongs to the doublet subspace, $|\psi\rangle = \psi_a|a\rangle + \psi_s|s\rangle$, with $|\psi_a|^2 + |\psi_s|^2 = 1$. The measurement of the current eigenvalue j then provides us with a probabilistic measure of $P_s = |\psi_s|^2$: while the result $j = 0$ appears with a probability $(2/3)P_s$, the current value $j = 1$ is realized with a probability $(1/3)P_s + P_a = 1 - (2/3)P_s$, from which the desired quantity P_s is easily derived within a multi-shot measurement scheme. In an experiment tracing the Rabi oscillations between the states $|a\rangle$ and $|s\rangle$ the specific time dependence $P_s(t) = \cos^2(\Omega_{\text{Rabi}}t)$ transforms into the probability difference $\mathcal{P}_{j=1}(t) - \mathcal{P}_{j=0}(t) = 1/3 - (2/3)\cos(2\Omega_{\text{Rabi}}t)$; the reduction in the amplitude is a consequence of the admixture of the third state $|0\rangle$.

The actual measurement of the current is carried out with the same (symmetric) measurement current configuration as discussed in the previous section. The only difference is that in the present measurement the current eigenvalues are proportional to $j = 1$ and $j = 0$ instead of ± 1 , i.e., the switching of (one of the two) junctions ‘n2-m1’, ‘n3-m2’ (or, depending on the sign of flux bias, ‘n2-m3’, ‘n3-m1’) is characteristic for a $j = 1$ eigenstate, whereas the absence of any switching corresponds to the $j = 0$ state.

V. CONCLUSIONS

The CH_4 molecule can be viewed as a molecular analogue to the tetrahedral superconducting structure with the same tetrahedral symmetry group. The non-Abelian character of this symmetry group is responsible for the natural appearance of degenerate states. However, contrary to the situation in atomic and molecular physics, where such degenerate levels usually correspond to excited states, the macroscopic device discussed here can be tuned such that the non-Abelian character of its symmetry group manifests itself in the appearance of a degenerate ground state. In order to do so, we have to bias the device, both electrically and magnetically, to the maximally frustrated point with half-flux $\Phi_0/2$ threading

each sub-loop and half-Cooper-pair charge e induced on each island. The ground state is a doublet equivalent to a spin-1/2 system in a vanishing magnetic field.

Given the above analogy to molecular physics, one may ask whether a splitting of the doublet ground state due to a Jahn-Teller type instability may appear in our system as well. In the superconducting tetrahedron this would correspond to a paramagnetic instability with a spontaneous breaking of time reversal symmetry: paramagnetic currents would lower the system energy due to their interaction with the self-generated magnetic field and the ground state doublet would split — the magnitude of this effect is determined by the magnetic inductance of the device which we have set to zero in our analysis above. However, in order to realize such an instability, the energy gain should be linear in the spontaneously generated flux; since our device exhibits only a quadratic dependence on flux, cf. (32), this type of instability is absent.

On a technical level, the superconducting tetrahedral qubit comes with a number of practically useful features: *i)* The weak quadratic sensitivity to electric and magnetic noise implies long decoherence times for this device, similar to the ‘quantronium’ discussed by Vion *et al.*⁷. At the same time, the quadratic dependence on bias allows for a manipulation via *ac*-fields rather than the usual *dc*-bias, hence the most dangerous low-frequency part of the noise spectrum can be blocked from the qubit via appropriate filters. *ii)* The degenerate ground state allows to avoid the appearance of phonon radiation during idle time³²: Assume a qubit with states $|0\rangle$ and $|1\rangle$ residing at different energies $E_0 \neq E_1$. A superposition state $|\Psi\rangle(t) = [\exp(-iE_0t/\hbar)|0\rangle + \beta \exp(-iE_1t/\hbar)|1\rangle]/\sqrt{1+|\beta|^2}$ will induce voltage oscillations $V = \hbar\dot{\varphi}/2e \propto (E_1 - E_0)/2e$ across the Josephson junction which couple to the underlying lattice via the piezo-electric effect. Hence, the junction acts as an antenna emitting phonons which contributes to the energy relaxation rate of the qubit. In our tetrahedral qubit, $E_1 = E_0$ and this loss channel is avoided during idle time. *iii)* The tetrahedral qubit can be fabricated with junctions of relatively large size. This is the consequence of a weak $\propto \exp[-\text{const.}(E_J/E_C)^{1/4}]$ rather than the usual $\propto \exp[-\text{const.}(E_J/E_C)^{1/2}]$ suppression of the qubit’s operational energy scale and entails two important advantages: first, less stringent requirements on the fabrication process and better junction uniformity, and second, an improved robustness of the qubit with respect to charge noise originating from fluctuating stray charges. The physical origin of this benevolent behavior is found in the huge classical ground state degeneracy originating from junctions with a simple $\propto \sin\varphi$ current-phase relation combined with a maximal magnetic frustration; this degeneracy then is lifted only due to quantum fluctuations^{15,16}. *iv)* The tetrahedral qubit admits a large variety of manipulation schemes — arbitrary manipulations of the effective ‘spin 1/2’ ground state can be implemented through either magnetic or electric bias fields. *v)* The quantum measurement can be performed with respect to different basis states and us-

ing either charge or flux bias. We have described schemes operating in the qubit eigenbasis and projective measurements onto the current basis. In the former setup, we have described detailed procedures for the detection of both ‘spin’ projections σ_z and σ_x . In the latter scheme, we have identified a high-quality measurement scheme for the operators σ_z and σ_y through appropriate charge bias; the flux bias scheme produces a non-ideal but acceptable setup for the measurement of σ_x . Proper rotation of the bias scheme by $\pm 2\pi/3$ provides a measurement of the corresponding rotated spin-components.

The above advantages seem worth the additional complexity of the device. Still, one may pose the question whether the same benefits can be implemented with a simpler device. E.g., the C_{3v} symmetry group of the symmetric three-junction loop²² also contains a two-dimensional representation and appropriate charging with $q_i = 1/3$ -charge per island produces a doublet ground state suitable for quantum computation. However, this simpler design does not exhibit the quadratic stability under charge noise — charge biasing one island reduces the symmetry to Z_2 with only one-dimensional representations and the doublet splits in linear order in δ_i^Q . On the contrary, charge biasing the tetrahedron re-

duces the symmetry from T_d to C_{3v} which still contains a two-dimensional representation. Indeed, the two complex conjugated states $|\pm\rangle$ react the same way to a charge bias δ_i^Q and hence the doublet splits only in quadratic order. This behavior, the indifferent response of the two ground state wave functions to a local perturbation is strongly reminiscent of the idea of topological protection, where the fault tolerance of the device is implemented on the hardware¹⁴ rather than the software level³³. The above symmetry arguments then show, that in order to benefit from a protected degenerate ground state doublet, the qubit design requires a certain minimal complexity; it seems to us that the tetrahedron exhibits the minimal symmetry requirements necessary for this type of protection and thus the minimal complexity necessary for its implementation.

We acknowledge discussions with Ch. Helm, A. Ioselevich, P. Ostrovsky, and M. Troyer, and financial support from the Swiss National Foundation (SCOPE, CTS-ETHZ), the Russian Ministry of Science, the program ‘Quantum Macrophysics’ (RAS), the RFBR grant 01-02-17759, and the NSF grant DMR-0210575. Numerical calculations have been carried out on the Beowulf cluster ASGAR at ETHZ.

-
- ¹ Y. Nakamura, Yu.A. Pashkin, and J.S. Tsai, *Nature* **398**, 786 (1999).
 - ² A. Shnirman, G. Schön, and Z. Hermon, *Phys. Rev. Lett.* **79**, 2371 (1997).
 - ³ D.V. Averin, *Solid State Commun.* **105**, 659 (1998).
 - ⁴ J.R. Friedman, V. Patel, W. Chen, S.K. Tolpygo, and J.E. Lukens, *Nature* **406**, 43 (2000).
 - ⁵ C.H. van der Wal, A.C.J. ter Haar, F.K. Wilhelm, R.N. Schouten, C.J.P.M. Harmans, T.P. Orlando, S. Lloyd, and J.E. Mooij, *Science* **290**, 773 (2000).
 - ⁶ I. Chiorescu, Y. Nakamura, C.P.M. Harmans, J.E. Mooij, *Science* **299**, 1869 (2003).
 - ⁷ D. Vion, A. Aassime, A. Cottet, P. Joyez, H. Pothier, C. Urbina, D. Esteve, and M. Devoret, *Science* **296**, 886 (2002).
 - ⁸ J.A. Jones, V. Vlatko, A. Ekert, and G. Castagnoli, *Nature* **403**, 869 (2000).
 - ⁹ L.M. Duan, J.I. Cirac, and P. Zoller, *Science* **292**, 1695 (2001).
 - ¹⁰ L.B. Ioffe, M.V. Feigel’man, A. Ioselevich, D. Ivanov, M. Troyer, and G. Blatter, *Nature* **415**, 503 (2002).
 - ¹¹ L.B. Ioffe and M.V. Feigel’man, *Phys. Rev. B* **66**, 224503 (2002).
 - ¹² B. Douçot, M.V. Feigel’man, and L.B. Ioffe, *Phys. Rev. Lett.* **90**, 107003 (2003).
 - ¹³ B. Douçot, L.B. Ioffe, and J. Vidal, *cond-mat/0302104*.
 - ¹⁴ A.Yu. Kitaev, *Annals of Physics* **303**, 2 (2003).
 - ¹⁵ H.G.B. Casimir, *Proc. K. Ned. Akad. Wet.* **51**, 793 (1948).
 - ¹⁶ J. Villain, R. Bidaux, J.P. Carton, and R. Conte, *J. Phys. (Paris)* **41**, 1263 (1980).
 - ¹⁷ A.M. Tsvelik *Quantum field theory in condensed matter physics* (Cambridge University Press, Cambridge UK, 1995). Chap. 17.
 - ¹⁸ M.V. Feigel’man, L.B. Ioffe, V.B. Geshkenbein, P. Dayal, and G. Blatter, *Phys. Rev. Lett.* **92**, 098301 (2004).
 - ¹⁹ D. Langbein, *Theory of Van der Waals forces* (Springer-Verlag, New York, 1974).
 - ²⁰ Y. Yu, S. Han, X. Chu, S. Chu, and Z. Wang, *Science* **296**, 889 (2002).
 - ²¹ J.M. Martinis, S. Nam, J. Aumentado, and C. Urbina, *Phys. Rev. Lett.* **89**, 117901 (2002).
 - ²² D.A. Ivanov, L.B. Ioffe, V.B. Geshkenbein, and G. Blatter, *Phys. Rev. B* **65**, 024509 (2002).
 - ²³ L.D. Landau and E.M. Lifshitz, *Quantum Mechanics* (Pergamon, Oxford, 1977), p. 184.
 - ²⁴ G. Blatter, V.B. Geshkenbein, and L.B. Ioffe, *Phys. Rev. B* **63**, 174511 (2001).
 - ²⁵ H. Tsunetsugu, *Phys. Rev. B* **65**, 024415 (2002).
 - ²⁶ M.V. Berry, *Proc. R. Soc. London A* **392**, 45 (1984).
 - ²⁷ F. Wilczek and A. Zee, *Phys. Rev. Lett.* **52**, 2111 (1984).
 - ²⁸ *Geometric Phases in Physics*, eds. A. Shapere and F. Wilczek (World Scientific, Singapore, 1989).
 - ²⁹ J. Clarke, T.L. Robertson, B.L.T. Plourde, A. García-Martínez, P.A. Reichardt, D.J. Van Harlingen, B. Chesca, K. Kleiner, Y. Makhlin, G. Schön, A. Shnirman, and F.K. Wilhelm, *Physica Scripta* **102**, 173 (2002).
 - ³⁰ A. Aassime, G. Johansson, G. Wendin, R.J. Schoelkopf, and P. Delsing, *Phys. Rev. Lett.* **86**, 3376 (2001).
 - ³¹ Y. Makhlin, G. Schön, and A. Shnirman, *Rev. Mod. Phys.* **73**, 357 (2001).
 - ³² L.B. Ioffe, V.B. Geshkenbein, Ch. Helm, and G. Blatter, to appear in *Phys. Rev. Lett.* (2004).
 - ³³ J. Preskill, *Fault-tolerant quantum computation. Introduction to quantum computation and information* (World Scientific, Singapore, 1998).